INPP4B drives lysosome biogenesis to restrict leukemic stem cell differentiation and promote leukemogenesis

Authors:

John F. Woolley[1,2,‡*], Keyue Chen[1], Golam T. Saffi[1], Gizem E. Genc[3], Daniel K.C. Lee[1], Irakli Dzneladze[2], Ruijuan He[2], Jonathan T.S. Chow[1], Martino M. Gabra[1], Meong Hi Son[1,2,§], Ché M.P. Melo[1], Candaice A. Newell[1], Aobo He[1], Erwin M. Schoof[2], Stephanie Z. Xie[2], Emily M. Mangialardi[1], Max Kotlyar[4], Ayesha Rashid[2], Miki. S. Gams[5,6], Jean Vacher[7], Cynthia J. Guidos[5,6], Igor Jurisica[4,8,9,10], John E. Dick[2,11,12], Roberto J. Botelho[3], Mark D. Minden[2,7], and Leonardo Salmena[1,2,13*]

Affiliations:

[1] Department of Pharmacology & Toxicology, University of Toronto, Toronto, Ontario M5S 1A8, Canada
[2] Princess Margaret Cancer Centre, University Health Network, Toronto, Ontario M5G 1L7, Canada
[3] Department of Chemistry and Biology, Ryerson University, Toronto, Ontario M5B 2K3, Canada
[4] Osteoarthritis Research Program, Division of Orthopedic Surgery, Schroeder Arthritis Institute, University Health Network; Data Science Discovery Centre for Chronic Diseases, Krembil Research Institute, University Health Network, Toronto, Ontario M5T 0S8, Canada.
[5] Developmental & Stem Cell Biology Program, Hospital for Sick Children Research Institute, Toronto, Ontario, Canada.
[6] Department of Immunology, University of Toronto, Toronto, Ontario, Canada.
[7] Institut de Recherches Cliniques de Montréal (IRCM), Département de Médecine, Université de Montréal, Montréal, Québec H2W 1R7, Canada
[8] Department of Computer Science, University of Toronto, Toronto, Ontario M5T 3A1, Canada
[9] Departments of Medical Biophysics, University of Toronto, Toronto, Ontario M5G 1L7, Canada
[10] Institute of Neuroimmunology, Slovak Academy of Sciences, Bratislava, Slovakia
[11] Department of Molecular Genetics, University of Toronto, Toronto, Ontario M5S 1A8, Canada
[12] Ontario Institute for Cancer Research, Toronto, Ontario M5G 0A3, Canada
[13] Lead Contact

Author list footnotes:

[‡]Present address: Department of Pharmacology & Therapeutics, Institute of Systems, Molecular and Integrative Biology, University of Liverpool, UK.

[§]Present address: Department of Pediatrics, Samsung Medical Center, Sungkyunkwan University School of Medicine, Seoul, Korea

*Correspondence: leonardo.salmena@utoronto.ca (L.S.)

Summary (148 words)

Signaling pathways that control vital features of leukemic stem cells including multipotency, self-renewal, clonal expansion and quiescence remain unclear. Emerging studies illustrate critical roles for lysosomes in hematopoietic and leukemic stem cell fate. By investigating INPP4B functions in AML, we discovered a signalling pathway that may drive 'stemness' in leukemia. We observed that *INPP4B* is highly expressed in hematopoietic progenitor, and leukemic stem cell populations. *Inpp4b*-deficeint hematopoietic stem cells have reduced long-term repopulation capacity, and *Inpp4b*-deficeint leukemias demonstrate increased disease latency, reduced leukemia initiating potential which is associated with a differentiated leukemic phenotype. Molecular analyses show that *Inpp4b*-deficient leukemias have compromised lysosomal gene expression, lysosomal content, and lysosomal activity. Our discovery of a novel pathway linking INPP4B, lysosomal biogenesis and leukemic stemness, provides a mechanism to explain the association of high *INPP4B* expression with poor AML prognosis, and highlights novel patient stratification strategies and LSC-specific leukemic therapies.

Keywords

AML; LSC; lysosome; differentiation; INPP4B

Introduction

Acute myeloid leukemia (AML) is an aggressive malignancy of the bone marrow characterized by dysregulated proliferation of immature myeloid cells and poor survival rates [1,2]. Most AML patients who receive intensive chemotherapy achieve a significant clinical response, however a majority will relapse within 5 years and succumb to their disease [1,2]. AML exists in a cellular hierarchy with leukemic stem cells (LSC) at the pinnacle that possess 'stemness' attributes including a capacity for self-renewal, multipotent differentiation, long-term clonal propagation and quiescence [3,4]. AML patients with more stem-like disease and greater LSC content have higher risk of relapse and worse clinical outcomes [5–8]. LSCs continuously sustain the hierarchy of malignant undifferentiated myeloid 'blast' cells that define AML and drive relapse [3,4]. Despite an increased understanding of the roles for 'stemness' in relapse and chemoresistance in AML over the past decades, the underlying molecular mechanisms remain unclear.

Phosphoinisitide-3-kinase (PI3K) pathway signaling is frequently high in AML blasts, however unlike most malignancies where the major genes in the PI3K/Akt pathway are frequently mutated, *PIK3CA*, *PTEN* and *AKT* are rarely affected with mutation and CNV frequencies below 0.5% [9,10]. PI3K/Akt activation in most AML can be explained by alterations in membrane-associated growth factor receptors [9,10]. We previously reported that expression of *Inositol Polyphosphate-4-Phosphatase Type II (INPP4B),* a lipid phosphatase that hydrolyzes phosphatidylinositol-3,4-bisphosphate [PtdIns(3,4)P_2] to generate phosphatidylinositol-3-monophosphate [PtdIns(3)P], is elevated in the leukemic blasts of approximately one quarter of all AML patients and is associated with poor prognosis [11]. Since both PI(3,4)P_2 is required for membrane recruitment and maximal activation of Akt, the PI(3,4)P_2 phosphatase function of INPP4B was predicted to be tumour suppressive [12–16]. Indeed, numerous studies have confirmed that INPP4B suppresses breast, ovarian, skin, and prostate cancer among others [17–21]. However, studies in AML [11,22–25] and other malignancies [26–29] demonstrate that INPP4B can have oncogene-like roles which promote the progression of cancer. These findings prompted us to investigate specific tumour-promoting roles of INPP4B in leukemogenesis. Herein we present lines of evidence illustrating a novel role for the phosphoinositide phosphatase INPP4B in the regulation of lysosomal properties, through which it controls leukemia stem cell maintenance and AML phenotypes.

Results

High levels *INPP4B* expression in AML are associated with leukemic stemness signatures

Analysis of overall (OS) and event-free survival (EFS) demonstrate that *INPP4B* transcript levels effectively stratify AML patients into poor survivorship groups with high *INPP4B* expression and favorable survivorship groups with low *INPP4B* expression (**Fig. 1A, B)** as previously demonstrated [11,23,30]. To shed light on cellular and molecular processes affected by *INPP4B* expression in AML, we identified the most significantly overrepresented gene ontologies associated with the top 200 genes

enriched in high *INPP4B* patient samples across several AML patient databases (**Supplementary Table 1)**. As expected, this analysis highlighted significant associations of high *INPP4B* expression with gene networks associated with phosphoinositide, PI3K and Akt signal transduction **(Fig. 1C)**. Notably, we also observed a significant association of high *INPP4B* expression with signaling networks related to leukemic stemness including hemopoiesis, stem cell proliferation, megakaryocyte differentiation, and hematopoietic progenitor cell differentiation (**Fig. 1C).** Given these associations, we explored the association of *INPP4B* expression with leukemic stemness by measuring specific enrichment of the LSC-17 signature, a prognostic score based on a 17-gene expression signature of LSCs to predict outcome in AML patients [7]. We observed a striking enrichment of the LSC-17 signature in patient samples with high INPP4B expression across all AML patient databases tested (**Fig. 1D, E & Supplementary Fig. 1 A, B**) [31–35]. To support these findings experimentally, assessment of *INPP4B* transcript levels in gene expression profiles from 227 AML patients' blast cells sorted based on the expression of CD34 and CD38 surface markers demonstrated highest levels in $CD34^{+}CD38^{-}$ populations and lower expression within other subpopulations (**Fig. 1F**), where $CD34^{+}CD38^{-}$ subpopulations are considered to be most highly enriched for LSC [7]. In keeping with the notion that LSC and their capacity for disease reconstitution is not defined exclusively on the basis of the CD34 and CD38 cell surface marker phenotypes, patient derived cell populations defined functionally through bone marrow transplant experiments [5,7] revealed that leukemic populations with disease initiating capacity (LSC^{+}) had higher levels of *INPP4B* expression compared to leukemic lineages that did not generate disease (**Fig. 1G**). Indeed, high *INPP4B* expression had an odds ratio of ~6 for association with functionally defined LSC^{+} populations (Chi-square *P*-value < 0.0001). These analyses of *INPP4B* gene expression in AML patient datasets, and subpopulations of leukemic progenitor populations represent the first evidence pointing to an association between *INPP4B* and leukemic stemness.

Hematopoietic stem and progenitor cell populations express elevated levels of *INPP4B*

Given our findings in LSCs, we investigated the existence of an underlying role for INPP4B in normal hematopoietic stemness. For this we first interrogated expression datasets derived from purified human [36–42] and mouse [43,44] hematopoietic stem cells (HSCs) and hematopoietic stem progenitor cell (HSPC) populations. Notably, expression of *INPP4B* was consistently observed to be highest in HSPC populations with the greatest pluripotency and self-renewal potential [eg. long-term (LT)-HSCs, short-term (ST)-HSCs and multipotent progenitor cells (MPPs)]; and progressively lower levels of expression were observed in the more committed progenitors and terminally differentiated myeloid lineage cells including granulocytes and monocytes (**Fig. 1H and Supplementary 1C**). Similarly, in murine hematopoietic cell populations, *Inpp4b* expression was highest in LT-HSCs and bulk HSCs, with lower levels found in lineage restricted HSPCs and terminally differentiated populations (**Fig. 1I and**

Supplementary 1D). These data provide compelling evidence that *INPP4B* expression is associated with hematopoietic stemness and may have a role in HSPC pluripotency (**Fig. 1J**).

Inpp4b deficiency leads to alterations in hematopoietic progenitor populations and function

To study *Inpp4b* function in HSPCs *in vivo*, we used the constitutive *Inpp4b*-knockout mouse model (*Inpp4b*$^{-/-}$) [45]. In our studies *Inpp4b*$^{-/-}$ and *Inpp4b*$^{+/-}$ mice were viable and born at the expected Mendelian frequencies, with no incidence of cancers nor premature lethality observed in C57BL/6 *Inpp4b*$^{-/-}$ or *Inpp4b*$^{+/-}$ mice up to 2 years of age, consistent with other published *Inpp4b* mouse models [46,47]. Gross hematological phenotypes in 6-10 week old *Inpp4b*$^{-/-}$ mice compared to *Inpp4b*$^{+/+}$ mice demonstrated no measurable differences in total bone marrow cellularity, circulating white blood cell counts, lymphocytes, monocytes, neutrophils, red blood cells and platelet numbers in peripheral blood (**Fig. Supplementary 2A,B**). However, flow cytometric analysis of HSPC populations from adult *Inpp4b*$^{-/-}$ mice (> 6 weeks of age) revealed a significant reduction in the number of LSK (Lin^{-}Sca-1^{+}c-Kit^{+}), short-term HSCs (ST-HSC; CD34^{+}CD150^{+}CD48^{-}LSK) and long-term HSC (LT-HSC; CD34^{-}CD150^{+}CD48^{-}LSK or EPCR^{+}LSK) (**Fig. 2A,B; Fig. Supplementary 2C,D**), and reduction in multipotent progenitors (MPP) that did not reach significance (**Fig. 2B**) relative to littermate *Inpp4b*$^{+/+}$ mice. Granulocyte monocyte progenitors (GMP) were significantly reduced, whereas megakaryocyte erythrocyte progenitors (MEP) were significantly increased in *Inpp4b*$^{-/-}$ bone marrow and no differences were observed in common myeloid progenitor (CMP) and lymphomyeloid-primed progenitor (LMPP) fractions **(Fig 2C)**. Together, these findings demonstrate a role for *Inpp4b* in HSPC homeostasis. Functional consequences of *Inpp4b*-deficiency on defining hallmarks of HSC were also evaluated using assays which measure self-renewal, differentiation, and long-term clonal propagation *in vitro* and *in vivo*. First, *in vitro* colony forming and self-renewal potential of bone marrow cells from *Inpp4b*$^{+/+}$ and *Inpp4b*$^{-/-}$ mice were assessed using colony-forming cell (CFC) assays with serial replating every seven days for a total of 4 weeks (**Fig. 2D**). Seven days after the initial plating, we observed no difference in the number of total colonies between *Inpp4b*$^{+/+}$ and *Inpp4b*$^{-/-}$ colony formation capacity. Upon re-plating, total colony numbers from *Inpp4b*$^{-/-}$ bone marrow were significantly reduced (day 14: 126 ± 8.4 *vs* 94 ± 8.2), with further marked reduction after the third plating (day 21: 105 ± 15.0 *vs* 14 ± 3.9) indicating a premature collapse of colony forming capacity of *Inpp4b*$^{-/-}$ bone marrow cells. The reduction in total colony numbers at day 14 in *Inpp4b*$^{-/-}$ specimens was a result of significantly decreased CFU-M colonies compared to other lineages (**Fig. Supplementary 2E**), suggesting that *Inpp4b*-deficiency leads to a defect in the differentiation of myeloid-committed precursors, particularly of the monocyte lineage. By day 21, premature collapse of all lineages in *Inpp4b*$^{-/-}$ progenitors was observed (**Fig. 2D, Fig. Supplementary 2E)**. Next, to measure a role for Inpp4b in the repopulation potential of HSCs *in vivo*, *Inpp4b*$^{+/+}$ and *Inpp4b*$^{-/-}$ mice were challenged with a myeloablation regimen of weekly i.p. injections of 5′-fluorouracil (5′-FU). Ki67 staining of sorted HSPCs (Lin^{-}Sca-1^{+}Kit^{+}) 48 hours after a single acute

treatment of 5′-FU revealed that *Inpp4b*$^{-/-}$ HSPCs had a significant increase in cycling HSPCs as compared to *Inpp4b*$^{+/+}$ HSPCs (**Fig. 2E**). Survival analysis demonstrated that *Inpp4b*$^{-/-}$ mice had significantly reduced overall survival compared to wild-type littermates upon serial myeloablation (mean survival 24 days *vs.* 28 days P = 0.008; **Fig. 2F**). These data suggest that the induction of replicative-stress in *Inpp4b*$^{-/-}$ HSPCs leads to aberrant hyperproliferation, which is coincident with premature lethality of *Inpp4b*$^{-/-}$ mice. Finally, a role for *Inpp4b* in the long-term repopulation capacity of HSPCs was measured through serial competitive transplant assays with *Inpp4b*$^{+/+}$, *Inpp4b*$^{+/-}$ and *Inpp4b*$^{-/-}$ bone marrow, where LT-HSC output was determined as the relative contribution of CD45.1 (competitor HSPCs) and CD45.2 (test HSPCs) to the myeloid lineage over 20 weeks post-transplant, in 3 consecutive *in vivo* repopulation experiments (**Fig. 2G,H, Fig. Supplementary 2F**). At 20 weeks after the primary competitive transplant we observed that *Inpp4b*$^{+/+}$ HSPCs, which contribute half (50%) of total myeloid cells, were outcompeted by *Inpp4b*$^{-/-}$ (78.5%) and *Inpp4b*$^{+/-}$ (70.0%) HSPCs. The increased contribution of the *Inpp4b*$^{-/-}$ and *Inpp4b*$^{+/-}$ cells at the first time point may be due to the increased rate of proliferation and failure of these cells to return to rest as observed in **Fig 2E**. At the end of the second transplant (44 weeks), *Inpp4b*$^{+/+}$ HSPCs continue to contribute approximately half (44%) of the total donor derived myeloid cells. However, in contrast to the earlier time point *Inpp4b*$^{-/-}$ HSPCs demonstrate a reduced reconstitution capacity at 27% and *Inpp4b*$^{+/-}$ HSPCs continue to outcompete *Inpp4b*$^{+/+}$ at 73% of total myeloid cells. However, at 64 weeks, both *Inpp4b*$^{+/-}$ and *Inpp4b*$^{-/-}$ bone marrow cells demonstrated a near-complete loss of contribution to the myeloid compartment compared to *Inpp4b*$^{+/+}$ bone marrow, indicating that *Inpp4b*-deficient HSCs have a reduced capacity for long-term hematopoietic repopulation.

***Inpp4b*-deficiency in *MLLAF9* leukemias leads to increased disease latency and altered differentiation status**

To investigate a direct role for *Inpp4b* in leukemogenesis *in vivo*, we generated a model of *Inpp4b*-deficient leukemia by transducing *Inpp4b*$^{-/-}$ LSK cells and control *Inpp4b*$^{+/+}$ LSK cells with MSCV-*MLL-AF9-Venus* retrovirus. Venus^{+}*Inpp4b*$^{-/-}$ and Venus^{+}*Inpp4b*$^{+/+}$ LSK cells were transplanted by tail vein injection into sub-lethally irradiated syngeneic host C57BL/6 mice to promote the development of primary leukemias **(Supplementary Fig. 3A**). Notably, all host animals transplanted with Venus^{+}*Inpp4b*$^{+/+}$ LSK cells succumbed to leukemia associated disease, however ~40% of Venus^{+}*Inpp4b*$^{-/-}$ LSK-transplanted mice survived beyond 300 days suggesting a decreased leukemia initiating potential associated with *Inpp4b*$^{-/-}$-leukemias (**Fig. 3A**). Secondary transplants **(Fig. 3B**) also demonstrated a significant increase in disease latency for the *Inpp4b*$^{-/-}$*-MLL-AF9* leukemia when compared to the *Inpp4b*$^{+/+}$*-MLL-AF9* leukemia (median survival of 76 *vs.* 41 days respectively; P = 0.0246). Furthermore, limiting dilution cell transplantation assays (LDA) revealed that *Inpp4b*$^{-/-}$*-MLL-AF9* leukemias have a significant decrease (1/147 *vs* 1/300 P = 0.0331) in leukemic initiating cell (LIC)

frequency (**Fig. 3C)**. Leukemia forming cell (LFC) assays carried out with primary *Inpp4b*$^{+/+}$ and *Inpp4b*$^{-/-}$ *MLL-AF9* leukemic cells demonstrated that *Inpp4b*-deficiency leads to a significant decrease in total leukemic colonies (**Fig. 3D)**. *Inpp4b*-deficiency also leads to a decrease in the percentage of type-I colonies (spherical with defined border, resembling primitive hematopoietic colony formation) countered by an increase in more differentiated type-II colonies (diffuse, lacking a defined border) (**Fig. 3E,F)** [48]. Finally, Wright–Giemsa staining of leukemic smears revealed a differentiated blast cell phenotype in *Inpp4b*$^{-/-}$ *MLL-AF9* as determined by an elevated proportion of multi-lobed, horseshoe-shaped, or diffuse nuclei (**Fig. 3G**). Only 16.9% of *Inpp4b*$^{+/+}$ *MLL-AF9* leukemia cells had a differentiated morphology, whereas 51.6% of *Inpp4b*$^{-/-}$*-MLL-AF9* leukemias had a differentiated phenotype. We used mass cytometry to determine and quantitate the differentiation status of *MLL-AF9* leukemias by evaluating the expression of 15 cell-surface hematopoietic differentiation markers. Compared to *wild-type* mouse bone marrow, mice burdened with *MLL-AF9* leukemias had very few erythroid and T/B lymphocytes (**Fig. Supplementary 3B**) and consisted predominantly of leukemic cells with CD11b^{+} CD16/32^{+} Gr1^{-} (**Fig. 3H-K)** cells that lacked Sca-1 and CD150 **(Fig. Supplementary 3C**), indicative of disease with myelomonocytic differentiation. Notably, a significantly higher percentage of *Inpp4b*$^{-/-}$ leukemic cells expressed Gr1 compared to Inpp*4b*$^{+/+}$ leukemias (**Fig. 3H,I)**, suggesting that *Inpp4b*-deficient leukemia is associated with granulocytic differentiation. On average, *Inpp4b*$^{-/-}$ leukemias also displayed more CD16/32^{+} CD117^{+} cells (**Fig. 3J,K**), but this difference was not significant. *Inpp4b*$^{-/-}$ and Inpp*4b*$^{+/+}$*-MLL-AF9* expressed significantly different levels of CD24, CD44 and CD16/32 (**Fig. 3L,M**) indicating that *Inpp4b* deficiency alters the differentiation status of *MLL-AF9* leukemias. Collectively, these data indicate that *Inpp4b*-deficiency in a *MLL-AF9* leukemia model generates leukemias with decreased leukemia initiating potential which is associate with decreased colony forming capacity, altered morphology and altered differentiation status analogous to *MLL-AF9* leukemia models reported previously [48]**.**

Identification of transcriptional networks perturbed by *Inpp4b* loss in leukemia

To determine the consequences of *Inpp4b* deficiency on molecular pathways and transcriptional networks in leukemia cells we performed RNA sequencing (RNA-seq) on freshly isolated bone marrow from mice burdened with *Inpp4b*$^{+/+}$ or *Inpp4b*$^{-/-}$ *MLL-AF9* leukemias. RNA-seq revealed a total of 5462 differentially expressed genes between *Inpp4b*$^{+/+}$ and *Inpp4b*$^{-/-}$ *MLL-AF9* leukemias (2434 downregulated, 3028 upregulated; FDR < 0.05; **Supplementary Fig. 4A, B**, **Supplementary Table 2).** To identify biological processes most significantly influenced by *Inpp4b* deficiency, we performed Gene Set Enrichment Analysis (GSEA**; Fig. 4A**) and gene ontology analysis (GO**; Fig. 4B**) on the differentially expressed gene list (**Supplementary Table 3**). Among the determination of many significantly enriched pathways, both analyses revealed highly significant associations with lysosomal gene sets (e.g., 64 out of 124 genes in the Kyoto Encyclopedia of Genes and Genomes (KEGG)

lysosomal gene signature; corrected *P*-value = 3.62×10^{-06}). Specific gene profiling demonstrated that a disproportionately large number of KEGG lysosomal gene transcripts were downregulated in *Inpp4b*$^{-/-}$ *MLL-AF9* gene profiles compared to *Inpp4b*$^{+/+}$ controls (**Fig. 4C**). Gene expression schematics generated by STRING-db, illustrated that the KEGG lysosome signature gene set could be subdivided into three protein interaction networks: trans-golgi network trafficking proteins, vacuolar ATPases and lysosome-active proteins and transporters. Although we observed loss of gene expression in all three groups, the most notable losses were strongly associated with lysosome-active proteins and transporters including several cathepsins (*Ctss, Ctsc and Ctsf*), lysosomal transporters (*Slc11a1*) and other proteases (*Lgmn, Psap, Lipa*) (**Fig. 4C, D**). To further support the association between *Inpp4b* expression with the KEGG lysosome signature (**Fig. 4E)**, we performed GSEA using independent lysosomal gene set curated from the Coordinated Lysosomal Expression and Regulation (CLEAR) network **(Fig. 4F)** and another from the harmonizome **(Fig. 4G)** with similar significant enrichment [49,50]. Together these results point to a role for Inpp4b in the regulation of lysosomal gene expression. Furthermore, to support the notion that *Inpp4b* deficiency in leukemia is associated with altered stemness and differentiation as demonstrated above (**Fig. 3**), we investigated the presence of changes in genes and networks associated with leukemic stemness or myeloid differentiation. GSEA revealed significant changes in the LSC17 gene signature, a myeloid cell development signature, and an osteoclast differentiation signature in *Inpp4b*-deficiency (**Supplementary Fig 4A-D**). These findings indicate that *Inpp4b*-deficiency in *MLL-AF9* leukemia significantly alters gene transcription networks associated with lysosome biology, myeloid stemness and myeloid lineage differentiation.

***INPP4B* expression in human AML is associated with lysosomal gene signatures**

By interrogating six AML patient datasets using GSEA, we identified the top 20 most enriched KEGG-defined gene sets associated with *INPP4B* expression (**Fig 5A-D, Supplementary Fig 5A, B)**. Notably, the lysosomal gene set, and other lysosome-related gene sets including glycosaminoglycan degradation and other glycan degradation were ranked among the top 20 most significantly enriched gene sets in all AML datasets tested (**Fig 5A-D, Supplementary Fig 5A, B)**. Enrichment scores for the KEGG lysosomal pathways were observed to be significant in TCGA, Valk, Verhaak, and Wouters AML patient datasets (**Fig 5E-H**) [31–33,35,82,85–87]. Furthermore, among the 121 genes which comprise the KEGG Lysosome gene set, 78 genes were classified as leading-edge genes (LEGs) in at least one of the TCGA, Verhaak, Valk and Wouters datasets, and a core set of 30 LEGs were present in all 4 datasets (**Fig 5I, J**). Together, the results of our analysis of public AML datasets provide further evidence that INPP4B plays a role in regulating the expression of lysosomal genes.

INPP4B promotes lysosomal gene expression without increasing nuclear translocation of TFEB

The expression level of many lysosomal transcripts was significantly associated with *INPP4B* status in murine leukemias and AML patients, suggesting a role in lysosome biogenesis. To identify a direct and causative role for INPP4B, we measured the effects of INPP4B overexpression on the levels of several core leading edge KEGG lysosomal genes **(Fig 5J)**. We observed that levels of *LAMP1*, *CTSB*, *CTSD*, *ATP6V1H*, *ATP6V1D*, and *MCOLN1* transcripts were significantly elevated in OCI-AML2 that overexpressed *INPP4B* **(Fig 6A)**. The promoter region of each of these, and many additional lysosomal genes share the coordinated lysosomal expression and regulation (CLEAR) consensus promoter element that is targeted by transcription factor EB (TFEB) [49]. We confirmed that *INPP4B* can positively induce lysosomal gene expression using a CLEAR reporter construct, where we observed a significant elevation of luciferase levels **(Fig 6B)**. Thus we hypothesized that *INPP4B* may promote TFEB activity upstream of CLEAR activation. Unexpectedly, INPP4B overexpression or knockout in OCI-AML2 did not alter the extent of TFEB nuclear localization in steady state, starved or serum restimulated conditions **(Fig 6C-F and Supplementary Fig 6A-C).** These data show that INPP4B increases lysosomal gene expression without increasing the nuclear translocation of TFEB. Further studies are required to elucidate the molecular interaction between INPP4B function and CLEAR gene activation.

INPP4B controls lysosomal content, function and sensitivity to lysosomal inhibition in AML cells

We next investigated a direct role for INPP4B in lysosome biology by measuring the consequences of *INPP4B* overexpression or knockout on lysosomal characteristics in AML cells. We first measured lysosome levels using Lysotracker Red (LTR) staining in AML cells. *INPP4B*-overexpression produced elevated levels of LTR fluorescence (**Fig. 7A**), whereas knockdown of *INPP4B* expression led to lower levels of LTR fluorescence (**Fig. 7B**). As a measure of lysosomal function, we assessed the proteolytic activity of lysosomes in our in OCI-AML2 cell models. Firstly, cathepsin B activity was measured using Magic Red, a lysosome permeable cresyl violet fluorophore substrate that becomes fluorescent when cleaved by cathepsin B. *INPP4B* overexpressing cells displayed significantly greater Magic Red fluorescence levels, whereas knockout of *INPP4B* reduced Magic Red fluorescence (**Fig. 7C,D**). Additionally, we used Dye Quenched-Bovine Serum Albumin (DQ-BSA)-Green, a sensor that is endocytosed and carried as cargo to lysosomes, where its bright fluorescence is activated by the acidic and highly proteolytic environment [52]. Leukemia cells incubated with DQ-BSA-Green were monitored hourly by flow cytometry. *INPP4B* overexpressing OCI-AML2 cells activated significantly greater levels of DQ-BSA-Green fluorescence compared to controls at each time point (**Fig. 7E**). Likewise, experiments conducted in *Inpp4b*$^{+/+}$ and *Inpp4b*$^{-/-}$ *MLL-AF9* leukemias for up to 8 hours showed that *Inpp4b*$^{-/-}$ leukemia cells had significantly lower levels of DQ-BSA-Green fluorescence throughout the time-course (**Fig. 7F**). Control experiments using fluorescent-tagged Dextran-Red to measure

endocytosis or trafficking rates demonstrated no difference in *INPP4B*-overexpressing or control OCI-AML2 cells, nor *Inpp4b*$^{+/+}$ and *Inpp4b*$^{-/-}$ *MLL-AF9* leukemia cells (**Supplementary Fig 7A-B**).

To further confirm a role for INPP4B in regulating lysosomal properties, we examined the consequences of lysosomal inhibition using the potent lysosomotropic agent Lys05 [53–55] in *Inpp4b*$^{+/+}$ and *Inpp4b*$^{-/-}$ *MLL-AF9* leukemia cells. Our tests with Lys05 included both viability and LFC assays. Firstly, a dose-response assessment in *MLL-AF9* leukemia cells *in vitro* demonstrated that *Inpp4b*$^{+/+}$ and *Inpp4b*$^{-/-}$ cells had similar sensitivity to the toxic effects of Lys05 (**Supplementary Fig 7C**). To specifically test the effects of Lys05 on colony forming capacity and colony differentiation we used sub-toxic concentrations as determined by dose response experiments. LFC assays showed that Lys05 reduced the colony forming potential of *Inpp4b*$^{+/+}$ *MLL-AF9* leukemia cells in a dose-dependent manner; but this effect was blunted in *Inpp4b*-deficient cells (**Fig. 7G)**. Thus, lysosomal inhibition reduces the colony forming capacity of *MLL-AF9* leukemia cells in an Inpp4b-dependent manner. We reasoned that this may be due to a differentiating effect of lysosomal inhibition on AML blasts. Thus, we performed independent LFC assays in Lys05-treated *Inpp4b*$^{+/+}$ *MLL-AF9* leukemia cells and specifically recorded the percentage of type I and type II colonies as a measure of colony differentiation. We observed that Lys05 treatment reduced the percentage of the more primitive type-I colonies and concomitantly increased the percentage of more differentiated type-II colonies in a dose dependent manner (**Fig. 7H)**. Altogether, these results indicate that INPP4B expression increases lysosomal content, promotes lysosomal function, and is necessary for the observed reduction in colony forming capacity and increased differentiation associated with lysosomotropic agents. Together our results suggest a model in which INPP4B promotes the development of AML with poor clinical characteristics by driving lysosomal content and function, which are vital to maintain leukemic stemness and prevent leukemic differentiation (**Fig 8**).

Discussion

Despite decades of basic and clinical research, relapse and chemoresistance remain a clinical predicament in AML. Increased stem-cell phenotypes and gene expression signatures in leukemic blasts are associated with relapse and chemoresistance in leukemia[5–8]. However underlying pathways that may serve as therapeutic targets remain undetermined. *INPP4B* overexpression was identified as an independent prognostic marker for poor disease outcome and a predictor of chemoresistance in AML [11,22–25]. Previous studies of have implicated pathways downstream of INPP4B as contributing to the AML progression and resistance including SGK3 signalling in NPM mutated AML [56] or blockade of apoptosis through IRF2–mediated autophagy [25,57,58]. INPP4B-associated chemoresistance was also linked to enhanced ATM-dependent DNA repair mediated by p65 nuclear translocation [24]. Our study presents the first evidence that INPP4B may promote poor disease outcome in AML through an ability

to promote leukemic stemness. By interrogating a number of human AML patient databases, investigating the consequences of *Inpp4b*-deficiency in murine hematopoiesis and leukemogenesis, combined with validation in AML cell line models, we discovered that (1) *INPP4B* expression is strongly associated with hematopoietic and leukemic stemness, (2) *INPP4B* expression is enriched in, and has critical functions in the repopulation capacity and leukemia initiating potential of HSCs and LSCs, respectively; (3) leukemias generated from *Inpp4b*-deficient cells have more differentiated phenotypes and exhibit increased disease latency compered to their *wild type* counterparts; (4) lysosome gene transcripts and lysosomal functions are regulated by INPP4B in AML; (5) Disruption of lysosome functions by either INPP4B depletion or direct pharmacological inhibition leads to leukemic differentiation (**Fig. 8**). Overall, by delineating INPP4B functions in AML, we have unveiled a novel signalling axis that drives 'stemness' in leukemia.

The first evidence to indicate a role for INPP4B in leukemic stemness was collected from a forty-four gene signature enriched in HSCs and LSCs [5]. Further analyses of purified leukemia cell populations and several AML patient datasets and revealed that *INPP4B* expression was associated with key features of LSCs in AML. These data pointed to a role for INPP4B in regulating stemness and differentiation. This notion was tested and confirmed in *Inpp4b*-deficient mice where long-term repopulation of HSCs was compromised. Notably, a marked increase in cycling and proliferation of *Inpp4b*-deficient HSPCs upon myeloablation and bone marrow reconstitution was observed prior to HSPC exhaustion phenotypes suggesting that Inpp4b may play a role in controlling stem cell cycling following replicative stresses. These findings are consistent with a model where *Inpp4b*-deficiency limits the ability of the HSC population to remain in quiescence, instead cells experience excessive proliferation, become more differentiated and ultimately suffer from long-term HSC exhaustion [37]. Analogously, *Inpp4b*$^{-/-}$ leukemias generated using the *MLL-AF9* oncogenic fusion protein, have a more differentiated AML phenotype and reduced leukemia initiating potential, further supporting a role for Inpp4b in maintaining 'stemness' and restricting differentiation. The association with leukemic stemness identifies INPP4B as a putative therapeutic target, with potential to compromise LSC self-renewal function and consequently drive differentiation of AML. However, given that INPP4B inhibition is not currently feasible, we sought to investigate processes downstream of INPP4B signaling with pharmacological potential. Expression profiling of *Inpp4b*$^{+/+}$ and *Inpp4b*$^{-/-}$ leukemias combined with gene network analyses revealed that the expression of key lysosomal genes including proteases and membrane transporters were strongly associated with *Inpp4b* status. This finding was corroborated in AML patient gene expression data and may represent rational candidate drug targets for AML therapy.

Lysosomes are membrane bound organelles that serve as a cell's main degradative centre [59,60]. More recently, lysosomes have been defined as key cellular sentinels of nutrient concentration and metabolic activity that have a critical role in integrating diverse signal transduction pathways including cell growth, division, differentiation and metabolism [61–64]. Importantly, studies implicating lysosomal

functions in stem cell maintenance are emerging. For instance, functional lysosomes in neuronal stem cells are needed to mitigate protein-aggregate accumulation, a consequence that would otherwise increase aging, reduce stem functions and lead to aberrant differentiation [65]. Studies in hematopoietic stem cells (HSC) demonstrated that quiescent HSCs are characterized by enlarged lysosomes which are crucial for the exquisite regulation of cell cycling [66]. Furthermore, lysosomes are asymmetrically distributed during division of stem cells, and thus predictive of future daughter cell fates [67]. Lysosomes also impact the fate of long-term HSCs through their ability to sense diverse cellular cues and coordinate signal transduction of pathways including cell cycling and metabolism [68]. In leukemia, increased lysosomal mass and biogenesis in leukemic progenitor cells selectively sensitizes AML cells to lysosomal inhibitors or disruptors [69,70]. More recently, key lysosomal signaling networks have been implicated in AML fate and differentiation [71]. Our work adds to this increasing body of knowledge by identifying an upstream regulatory pathways that can modulate lysosomal activity and thereby promote AML stemness.

Rogers *et al*. recently showed that INPP4B directly enhances late endosome/lysosome formation and drives cell proliferation and tumor growth in *PIK3CA*-mutant ER^+ breast cancers [29]. This was attributed to a mechanism whereby INPP4B-mediated $PI(3,4)P_2$ to PI(3)P conversion on late endosomes promotes Wnt/β-catenin signaling. Aberrant Wnt/β-catenin signaling has been linked with hematological malignancies, and specifically in AML patients increased WNT pathway signaling correlates with adverse clinical outcomes [72,73]. Our analyses did not reveal significant associations of INPP4B expression with WNT pathway signatures, although we did not validate that negative result, focussing instead on the positive link to lysosomal activity. In our studies, leukemic cell models with INPP4B overexpression and INPP4B depletion demonstrated that INPP4B can regulate lysosomal homeostasis through regulation of lysosomal gene expression and thereby increase lysosomal content, and the proteolytic capacity of lysosomes. Together, the study by Rogers *et al*. and our work indicate that INPP4B may have both direct and indirect roles in promoting lysosome content and function, respectively.

Lysosomes have emerged as an intriguing organelle with effects on the initiation, progression and therapy of cancer. It is now clear that lysosomal functions can contribute to several cancer hallmarks, including proliferation, altered metabolism, invasion and metastasis among others [74]. In leukemia and hematopoiesis, lysosomes can influence stemness and differentiation, a newly proposed cancer hallmark [75]. Given their pleiotropic roles in cancer cell biology, lysosomes have become an attractive target for cancer therapy [74]. Critically, lysosomes have also been implicated in chemoresistance through a lysosomal sequestration mechanism which is triggered by transcriptional lysosomal biogenesis [76]. Our observations with INPP4B in AML are resonant with the activation of transcriptional lysosome biogenesis which promote cancer progression, restricted leukemic differentiation and chemoresistance. Thus it is tempting to propose that lysosomal inhibition may

compromise AML by promoting LSC differentiation and simultaneously combat chemotherapy resistance. Moreover, in addition its ability to predict poor disease in AML, *INPP4B* expression may also serve as a biomarker of response to lysosomal inhibition in line with the notion that lysosomes in AML cells are bigger in size which could make AML cells more susceptible towards lysosomal disruption than normal cells [69,70].

Overall, our findings highlight a novel pathway linking INPP4B, lysosomal function and leukemic stemness. This new model provides an explanation for the ability of INPP4B to promote AML aggressiveness. These new data also underscore the utility of INPP4B as a biomarker of aggressive AML and provide a rationale to explore INPP4B and its associated function in lysosome biology as novel strategies to target LSC and AML

Acknowledgments

We thank all current and past members of the Salmena and Minden labs for technical assistance and critical discussions. We specifically thank Rod Bremner, Robert C. Laister for critical advice and editing, Norman Iscove for technical counsel; Johannes Zuber for *pMSCV-MLL-AF9-IRES-mVenus* plasmid; Lev Kats for invaluable advice and reagents;. L.S. is the recipient of a Tier II Canada Research Chair (CRC) and was supported through the Human Frontier Career Development Program (HFSP) Award. This work was supported in part by funds from the Department of Pharmacology and Toxicology and Temerty Faculty of Medicine, University of Toronto and awards from Canada Foundation for Innovation (CFI- #33505); The Natural Sciences and Engineering Research Council of Canada (NSERC-RGPIN-2015-03984); Leukemia and Lymphoma Society of Canada (LLSC-Operating Grant #317359; Operating Grant #422332); Acute Leukemia Translational Research Initiative through funding provided by the Ontario Institute for Cancer Research and Government of Ontario; Leukemia Research Foundation (LRF-New Investigator Award #169456), and Canadian Institutes for Health Research (CIHR-Operating Grant #149032; Operating Grant #399716) awarded to L.S. This work was supported in part by funds from CIHR (MOP# 123343) awarded to J.V. Computational analyses were supported in part by funds from NSERC (# 203475), CFI (#225404, #30865), Ontario Research Fund (RDI #34876), IBM and Ian Lawson van Toch Fund awarded to I.J. R.J.B. is a recipient of a Tier II CRC, and this work was supported in part by the NSERC (RGPIN-2015-05489 and RGPIN-2020-043343).

Author Contributions

J.F.W., K.C., G.G., D.K.C.L., G.T.S., E.M.S., S.Z.X. M.H.S., M.S.G, R.H., A.R. and L.S. performed experiments. D.K.C.L., M.G., M.K., I.D. and I.J. performed bioinformatic analyses. J.V. generated *Inpp4b* mouse models. C.J.G, J.E.D., R.B., and M.D.M. provided critical reagents, mentorship, and expertise. J.F.W. and L.S. conceived the project, planned the study, and wrote the paper. L.S. secured funding for this study. All authors read and approved the text.

Declaration of Interests

All other authors declare no competing interests.

Figure Titles and Legends

Figure 1. High levels *INPP4B* expression are associated with stemness signatures in leukemia and hematopoietic progenitor cells. **A.** Kaplan Meier analysis of overall survival in *INPP4B*^{high} *vs*. *INPP4B*^{low} AML patients from Verhaak dataset. **B.** Kaplan Meier analysis of event free survival in *INPP4B*^{high} *vs*. *INPP4B*^{low} AML patients from Verhaak dataset. **C.** Enriched terms related to phosphatidylinositol signaling or the hematopoietic compartment stem cells were highlighted in a chord diagram that was generated with the circlize R package (24930139). **D.** Heatmaps of LSC-17 gene expression in the Verhaak AML patient dataset, ranked by INPP4B expression (INPP4B-high quartile highlighted dark blue). **E.** Gene set enrichment analysis (GSEA) enrichment plot of the LSC-17 gene set in the Verhaak AML patient dataset ranked by *INPP4B* AML expression. **F**. Expression of *INPP4B* from 227 AML patient-derived samples sorted based on the expression of combinations of CD34 and CD38 surface markers. **G.** *INPP4B* expression in 278 sorted fractions characterized as LSC^{+} and LSC^{-} enriched by their engraftment potential into NOD/SCID mice. **H.** Relative expression of *INPP4B* in human hematopoietic stem and progenitor cells. **I**. Relative expression of *Inpp4b* in murine hematopoietic stem and progenitor cells. **J**. Schematic depicting *INPP4B* expression in the haematopoietic hierarchy (high = dark blue, low = light blue).

Figure 2. *Inpp4b*-deficiency reduces repopulation capacity of hematopoietic progenitors. **A.** Representative pseudocolour dot-plot and contour plot from immunophenotyping of the adult bone marrow niche in *Inpp4b*$^{+/+}$ and *Inpp4b*$^{-/-}$ mice. **B.** Bone marrow stem cell fractions and (**C)** bone marrow progenitor fractions from age- and sex-matched adult *Inpp4b*$^{+/+}$ and *Inpp4b*$^{-/-}$ mice, shown as a percentage of total bone marrow monocuclear cells. **D.** Total colony counts from weekly serial replating of total bone marrow from age- and sex-matched *Inpp4b*$^{+/+}$ and *Inpp4B*$^{-/-}$ mice (*n*=6, ± S.E.M.). **E.** Cell cycle analysis in sorted LSK cells, 48 hours after acute myeloablation with single 5'-fluorouracil treatment, measured by intracellular Ki67 level and flow cytometry (*n*=5, ± S.E.M.). **F**. Kaplan-Meier survival analysis after serial myeloablation (5'-fluorouracil, weekly i.p.) of age- and sex-matched *Inpp4b*$^{+/+}$ and *Inpp4B*$^{-/-}$ mice (*n*=10). **G.** Schematic describing competitive transplant experiments. **H.** Relative contribution of *Inpp4b*$^{+/+}$, *Inpp4b*$^{+/-}$ and *Inpp4b*$^{-/-}$ long term HSCs to the regeneration of the myeloid populations in three consecutive competitive transplant experiments (*n*=10, ±S.E.M.).

Figure 3. *Inpp4b*-deficient *MLL-AF9* cells have a decreased leukemogenic potential and have a more differentiated phenotype. **A.** Kaplan-meier survival analysis of primary Venus^{+}-*MLL-AF9* leukemias generated from *Inpp4b*$^{+/+}$ and *Inpp4B*$^{-/-}$ mouse LSK cells (*n*=10). **B.** Kaplan-meier survival analysis of secondary *MLL-AF9* leukemias generated by transplantation of cells from *Inpp4b*$^{+/+}$ and *Inpp4b*$^{-/-}$ *MLL-AF9* leukemia blasts (*n*=6). **C.** Limiting dilution assay (LDA) of *Inpp4b*$^{+/+}$ (dark blue (*n*=12)) and *Inpp4b*$^{-/-}$ *MLL-AF9* (light blue (*n*=12)) leukemia cells (1000, 250, 100, and 25 cells) into host

wildtype C57BL/6 mice. **D.** Total and percentage colony counts in LFC assays from *Inpp4b*$^{+/+}$ and *Inpp4B*$^{-/-}$ murine *MLL-AF9* leukemia blasts (*n*=8, ±S.E.M.). **E** Proportion of undifferentiated and differentiated leukemic blasts from *Inpp4b*$^{+/+}$ (*n*=8, ±S.E.M.). **F.** Representative image of type-I and type-II colonies from secondary *MLL-AF9* leukemia cells. **G.** Representative images of Wright–Giemsa staining of leukemic blasts from *Inpp4b*$^{+/+}$ and *Inpp4b*$^{-/-}$ *MLL-AF9* terminal leukemias; (U) undifferentiated and (D) differentiated (*n*=3, ±S.E.M.; left). **H,I.** Contour plots (10% probability) show CD11b versus Gr1 expression on live singlets from *Inpp4b*$^{+/+}$ versus *Inpp4b*$^{-/-}$ *MLL-AF9* leukemia samples compared to WT BM cells (representative of n=3/group). Scatter graph shows the % CD11b^{+} Gr1^{+} cells in each AML type. Two-tailed t-test with Welch's correction, *P* = 0.001. **J,K.** Contour plots show CD16/32 versus CD117 expression on CD11b^{+} Gr1^{-} cells from representative *Inpp4b*$^{+/+}$ and *Inpp4b*$^{-/-}$ *MLL-AF9* leukemia samples. Scatter graph shows the % CD16/32^{+} CD117^{+} cells in each type of AML. Two-tailed t-test with Welch's correction, *P* = 0.1726. **L.** Multiple unpaired t-tests with Welch's correction. Multiple comparisons corrected by False Discovery Rate using the 2-stage step-up method of Benjamini, Krieger and Yekiuteli. *, Q=0.03 for each comparison shown. **M**. Heatmap visualization of the median metal intensity (MMI) of the indicated markers on CD11b^{+} Gr1^{-} cells from each type of AML. Values for each marker were calculated as arcinsh (MMI(*x*)/□scale_argument)-□arcsinh (*control* /scale_argument) where *x* is the sample value, *control* is the lowest value for the marker across all samples, and scale argument=5.

Figure 4. *Inpp4b* expression is associated with lysosomal gene sets. **A**. Top 20 enriched KEGG gene sets in *Inpp4b*$^{+/+}$ and *Inpp4b*$^{-/-}$ *MLL-AF9* leukemia blast cells determined using GSEA. **B.** Top 20 enriched KEGG pathways from significantly upregulated genes (log-fold-change > 1, FDR < 0.05) in *Inpp4b*$^{-/-}$ MLL-AF9 leukemia blast cells were determined using the DAVID analysis tool. **C.** Heat map of differentially expressed KEGG Lysosome genes from *Inpp4b*$^{+/+}$ and *Inpp4b*$^{-/-}$ *MLL-AF9* leukemia blast cells (upregulated in red, downregulated in blue). **D.** STRING-db analysis of differential expression of KEGG Lysosome genes from *Inpp4b*$^{+/+}$ and *Inpp4b*$^{-/-}$ *MLL-AF9* leukemia blast cells. **E.** Gene set expression analysis (GSEA) for Lysosome pathway genes in *Inpp4b*$^{-/-}$ *MLL-AF9* leukemia blast cells witt the KEGG Lysosome gene set; (**F)** Lysosomal proteins gene set; (**G**) Harmonizome (Amigo) lysosome gene set.

Figure 5: A Lysosome gene set is enriched in patients with low levels of INPP4B. Histograms of the top 20 enriched KEGG gene sets in *INPP4B*-low patients from the (**A)** TCGA, (**B)** Valk (**C)** Verhaak and (**D**) Wouters AML patient datasets ranked by normalized enrichment score (NES). GSEA enrichment plots of KEGG Lysosome geneset demonstrating significant enrichment with INPP4B expression in (**E)** TCGA, (**F)** Valk (**G)** Verhaak and (**H**) Wouters AML patient datasets. **I.** Venn diagram illustrating the number of genes from the KEGG lysosome gene set that contribute to the leading-edge

subset in the four AML datasets. **J.** Table of the 30 common core enriched lysosome genes among the four AML datasets.

Figure 6: INPP4B promotes expression of lysosomal genes. Representative Western blots demonstrating (**A**) overexpression and (**B**) knockdown of INPP4B protein levels in OCI-AML2 cells. **C**. qRT-PCR analysis of lysosome gene expression in OCI-AML2 cells normalized against Actb. Shown is mean ± SEM from three independent experiments. **D.** HEK293T cells overexpressing control or INPP4B constructs were co-transfected with pGL3 4X-CLEAR-Firefly reporter and CMV-promoter Renilla luciferase internal control and quantitated as the ratio of Firefly to Renilla. **E,G.** OCI-AML2 cells in the steady state, FCS starved, or starved and FCS fed conditions were immunostained for TFEB and (**F,H**) analyzed for nuclear/cytosol TFEB intensity.

Figure 7: INPP4B regulates lysosomal biology in leukemia cells. *INPP4B* overexpressing (**A**) and *INPP4B* knockout (**B**) OCI-AML2 cells were labelled with 1uM lysotracker red were imaged by microscopy and quantitated using flow cytometry. *INPP4B* overexpressing (**C**) and *INPP4B* knockout (**D**) OCI-AML2 cells were labelled with Magic Red-cathepsin B were imaged by microscopy and quantitated using flow cytometry. Scale bar: 15 µm. **E.** Inducible-INPP4B OCI-AML2 cells were treated without or with doxycycline (100mg/mL) and incubated with DQ-BSA-Green™ and fluorescence was monitored by flow cytometry hourly, for up to 6 hours. Representative flow cytometry histograms displayed. **F.** *Inpp4b*$^{+/+}$ and *Inpp4B*$^{-/-}$ *MLL-AF9* leukemia blasts were incubated with DQ-BSA-Green™ and fluorescence was monitored by flow cytometry hourly, for up to 8 hours. Representative flow cytometry histograms displayed. **G.** *Inpp4b*$^{+/+}$ and *Inpp4B*$^{-/-}$ *MLL-AF9* leukemia blasts were plated in the LFC assay in the presence of Lys05 at indicated dose for 7 days and monitored for total colony counts or (**H)** percentage of type I and type II colonies. *Inpp4b*$^{+/+}$ *MLL-AF9* leukemia blasts were plated in the LFC assay in the presence of Lys05 at indicated dose for 7 days. Data represent ± SEM from at least three independent triplicate experiments with at least 10,000 events per condition. Students *t*-test or ANOVA and post-hoc analysis are displayed with *$P < 0.05$, ** $P < 0.01$, *** $P < 0.001$, **** $P < 0.0001$ compared to indicated control condition.

Figure 8: Model of INPP4B function in leukemia stem cells and leukemic blasts.

STAR Methods

Key Resources Table

REAGENT or RESOURCE	SOURCE	IDENTIFIER
Antibodies		
Anti-mouse lineage Cocktail	Biolegend	133313
anti-mouse CD45.1 PE	Biolegend	110708
anti-mouse CD45.2 FITC	Biolegend	109806
anti-mouse Ly-6A/E PE/Cyanine7	Biolegend	108114
anti-mouse CD150 PE	Biolegend	115904
anti-mouse CD48 BV 421™	Biolegend	103427
anti-mouse CD117 APC	Biolegend	105812
anti-mouse CD16/32 BV 510™	Biolegend	101333
anti-mouse CD34	BD Pharmingen™	560238
anti-mouse/human CD11b PE/Cyanine7	Biolegend	101216
anti-mouse Ly-6G/Ly-6C PE/Cyanine5	Biolegend	108410
Anti-mouse EPCR PE	Biolegend	141503
Anti-mouse Ki67 FITC	Biolegend	652410
Anti-mouse Gr1, Ly6G/C; 141 Pr; Clone RB6-8C5	Guidos lab, in house	
Anti-mouse CD11b, Itgam; 148 Nd; M1/70	Guidos lab, in house	
Anti-mouse CD19; 149 Sm;	Guidos lab, in house	

Clone 1D3		
Anti-mouse CD24; 150 Nd; Clone M1/69	Guidos lab, in house	
Anti-mouse CD3e; 152 Sm; Clone 145-2C11	Guidos lab, in house	
Anti-mouse TER-119, Ly76; 154 Sm; Clone TER-119	Guidos lab, in house	
Anti-mouse CD16/32; 155 Gd; Clone 2.4G2	Guidos lab, in house	
Anti-mouse CD45; 156 Gd; Clone 30-G12	Guidos lab, in house	
Anti-mouse Flt3, CD135; 162 Dy; Clone A2F10.1	Guidos lab, in house	
Anti-mouse Sca1, Ly-6A/E; 164 Dy; Clone E13-161.7	Guidos lab, in house	
Anti-mouse CD117, ckit; 166 Er; Clone 2B8	Guidos lab, in house	
Anti-mouse CD150, SLAM; 167 Er; Clone TC15-12F12.2	Guidos lab, in house	
Anti-mouse CD44; 171 Yb; Clone IM7	Guidos lab, in house	
Anti-mouse MHC class II; 174 Yb; Clone M5/114.15.2	Guidos lab, in house	
Anti-mouse B220; 176 Yb; Clone RA3-6B2	Guidos lab, in house	
Anti-human TFEB	Cell Signaling Technology	4240
Anti-human INPP4B	Cell Signaling Technology	14543S

Anti HDAC2	Cell Signaling Technology	2540S
Anti b-Actin	Cell Signaling Technology	4967
Chemicals, Peptides, Recombinant Proteins		
Ammonium Chloride	Stem Cell Technologies	07850
Mouse Recombinant IL-3	Stem Cell Technologies	78042
Mouse Recombinant IL-6	Stem Cell Technologies	78052
Mouse Recombinant SCF	Stem Cell Technologies	78064
MethoCult™ GF M3434	Stem Cell Technologies	03444
5’ Fluorouracil	Gift from Mark Minden	N/A
Cytarabine	Gift from Mark Minden	N/A
Critical Commercial Assays		
Mouse Cell Depletion Kit	Milteny Biotec	130-104-694
LS Columns	Milteny Biotec	130-042-401
RNeasy Mini Kit	Qiagen	74104
DQ™ Green BSA	Invitrogen/Thermo Fisher	D12050
Lysotracker	Invitrogen/Thermo Fisher	L7528
Dextran, Alexa Fluor™ 647	Invitrogen/Thermo Fisher	D22914
Cathepsin B Magic Red	Abcam	ab270772
Experimental Models: Organisms/Strains		
C57BL/6	Charles River Canada	Strain Code: 027
B6.SJL-PtprcaPepcb/BoyJ (CD45.1) mice	The Jackson Laboratory	Stock No: 002014

Inpp4b$^{-/-}$ mice	Jean Vacher, IRCM	Ferron *et al.* 2011

Resource Availability

Lead Contact: Further information and requests for resources and reagents should be directed to and will be fulfilled by the Lead Contact, Leonardo Salmena (leonardo.salmena@utoronto.ca).

Materials Availability: This study did not generate new unique reagents.

Data and Code Availability: The RNA sequencing data will be made available at Gene Expression Omnibus. All other datasets generated in this study are available within the paper or from the lead contact upon reasonable request.

Experimental Model and Subject Details

Mice. *Inpp4b*$^{-/-}$ mice kindly provided by Jean Vacher (Institut de Recherches Cliniques de Montréal) and were crossed into the C57BL/6 and genotyped as previously described [45]. C57BL/6 wild-type mice were bred and housed at the University Health Network/Princess Margaret Cancer Center and the Division of Comparative Medicine Facility at the University of Toronto. B6.SJL-Ptprca Pepcb/BoyJ (CD45.1) mice were purchased from The Jackson Laboratory (Bar Harbor, Maine, USA). All animal experiments were performed in accordance with national and institutional guidelines approved by the Canadian Counsel on Animal Care and approved by the University Health Network Animal Care Committee and the Division of Comparative Medicine at the University of Toronto.

Method Details

Gene expression data. Genome-wide expression data from The Cancer Genome Atlas (TCGA)-LAML dataset was downloaded from the ICGC database (https://icgc.org/). Normalized microarray data from the Herold (GSE37642-GPL570), Klein (GSE15434), Metzeler (GSE12417-GPL570), Valk (GSE1159), Verhaak (GSE6891), Wouters (GSE14468), Laurenti (GSE42414, GPL14951), Notta (GSE76234), Novershtern (GSE24759), Pietras (GSE68529), Rapin (GSE42519) and Lara-Asiato (GSE60101) datasets were downloaded from the GEO database (https://www.ncbi.nlm.nih.gov/geo/). GO analysis was performed using The Database for Annotation, Visualization and Integrated Discovery [DAVID; [77]]. The top 200 enriched genes in INPP4B^{high} patients from the TCGA, Verhaak, Wouters, Herold, Klein and Metzeler datasets were submitted to the DAVID analysis tool to identify enriched GO Biological Processes terms [77,78]. Enriched terms related to Phosphatidylinositol signaling or the hematopoietic compartment, and the corresponding datasets were highlighted in a chord diagram that was generated with the circlize R package [79].

Immunophenotyping of *Inpp4b*$^{-/-}$ mice. Total bone marrow was extracted from the hind legs of *Inpp4b*$^{+/+}$, *Inpp4b*$^{+/-}$ and *Inpp4b*$^{-/-}$ mice by crushing into ice-cold Iscove's Modified Dulbecco's Medium (IMDM) medium. RBC lysis was performed using standard ammonium chloride procedure. Total bone marrow mononuclear cell (MNCs) were stained for surface marker expression in PBS. 2mM EDTA, 2% FBS for 90 minutes at 4°C. The following antibody cocktails were used: anti-mouse CD3 (145-2C11), anti-mouse CD45R/B220 (RA3-6B2, anti-mouse CD11b (M1/70), anti-mouse Erythroid marker (TER-119), anti-mouse Ly-6G (RB6-8C5), anti-mouse CD34 (RAM34), anti-mouse Flk2 (A2F10), anti-mouse c-kit (2B8), anti-mouse Sca1 (D7), anti-mouse CD150 (TC15-12F12.2), anti-mouse CD48 (HM48-1), anti-mouse CD201/EPCR (eBio1560). All antibodies were obtained from eBiosciences, BD Pharmingen or Biolegend. Cells were analysed on a LSR Fortessa X20 (BD Biosciences). Total blood counts for Age- and sex-matched *Inpp4b*$^{+/+}$ and *Inpp4b*$^{-/-}$ mice (n=10) were performed using a VetScan HM5 (Abaxis) by the Division of Comparative Medicine (University of Toronto).

***In vitro* CFU Assays of *Inpp4b*$^{-/-}$ bone marrow.** To determine the re-plating ability of HSPCs *Inpp4b*$^{+/+}$ and *Inpp4b*$^{-/-}$ we plated bone marrow from age- and sex-matched mice in Methocult GF M3434 (Stem Cell Technologies) according to the manufacturer's instructions. Briefly, total mouse bone marrow MNCs were flushed from long bones into IMDM medium. RBCs were lysed in ammonium chloride solution and cells were resuspended in IMDM. 2 x 10^4 cells were plated onto 35-mm dishes and incubated at 37°C, 5% CO_2 for 7-days. After 7-days colonies were counted and scored. 2 x 10^4 cells were re-plated onto fresh methocult every 7 days and counted, until exhaustion.

5'-FU Treatment. Age- and sex-matched *Inpp4b*$^{+/+}$ or *Inpp4b*$^{-/-}$ mice were treated with 5'-FU (150mg/kg in saline, i.p.) or saline control, once weekly. Survival analysis was performed by the Kaplan-Meier method. Separately, LSK cells were sorted 48-hours after treatment with a single dose of 5'-FU from age- and sex-matched *Inpp4b*$^{+/+}$ and *Inpp4b*$^{-/-}$ mice. These LSK cells were then fixed, and cycling was assessed by flow cytometry measurement of Ki67 levels.

Competitive Transplant of *Inpp4b*$^{-/-}$ bone marrow. Lethally irradiated C57BL/6-CD45.1 congenic mice were reconstituted with bone marrow MNCs from age- and sex-matched *Inpp4b*$^{+/+}$ or *Inpp4b*$^{-/-}$ mice (CD45.2), in competition with bone marrow MNCs from C57BL/6-CD45.1 mice. Competitive transplants were carried out in a 1:1 ratio, with 1 x 10^6 cells from each combined prior to injection. Reconstitution of donor-derived cells (CD45.2) was monitored by staining blood cells with mAbs against CD45.2, CD45.1, Mac-1, and Gr-1. For the serial transplantation analysis, bone marrow cells (1×10^6) were obtained from recipient mice at 20 weeks post-transplantation and transplanted into a second set of lethally irradiated mice. The ratio of 1:1, Cd45.1:CD45.2 was re-established prior to secondary transplant. Subsequent transplants were performed in the same manner.

***MLL-AF9* AML Models.** *MLL-AF9* expressing cells were generated by retroviral transduction of murine bone marrow progenitors. Briefly, bone marrow was flushed from the long bones of 10-week-old *Inpp4b*$^{+/+}$ and *Inpp4b*$^{-/-}$ mice. From these total bone marrow preparations, 2 x 10^6 LSK cells were sorted and grown for 24 hours in IMDM supplemented with 20 ng/ml SCF, 10 ng/ml IL-6 and 10 ng/ml IL-3 (Gibco). *Inpp4b*$^{+/+}$ and *Inpp4b*$^{-/-}$ LSK were each retrovirally transduced with pMSCV-*MLL-AF9*-IRES-mVenus. 24 hours post retroviral transduction, 2 x 10^5 Venus$^+$ cells were transplanted to sub-lethally irradiated (4.5Gy) donor C57BL/6 mice to generate primary leukemias [80]. Subsequent transplantation of mVenus$^+$ cells from mice with terminal leukemias were performed with 250 cells and designated as secondary leukemia assays. *In vitro* leukemia forming cell (LFC) assays were performed in IMDM medium with 2% methylcellulose, supplemented with 20 ng/ml SCF, 10 ng/ml IL-6 and 10 ng/ml IL-3 (Stem Cell Technologies). Cytological analysis of blood and bone marrow smears from *Inpp4b*$^{+/+}$ and *Inpp4b*$^{-/-}$ leukemic mice was done by Wright-Giemsa staining (Sigma). For limiting dilution transplantation assays (LDA), *MLL-AF9* leukemia cells were injected at defined doses (equivalent to 10, 25, 50, 100, and 1000 blast cells) into 8-week-old female C57BL/6 mice. LSC frequency was estimated using the online tool ELDA (http://bioinf.wehi.edu.au/software/elda/index.html) [81].

Mass Cytometry. Purified mAbs were conjugated with heavy metals by the Flow and Mass Cytometry Facility, The Hospital for Sick Children. Murine AML blasts were counted and 2 x10^6 cells for each sample were stained for cell surface markers in staining media (PBS containing 1% BSA and 0.02% NaN3) for 30 minutes at 4C. Cells were washed with protein-free PBS, stained with 1 mmol/L cisplatin for 5 minutes at room temperature, fixed using the transcription factor buffer set (BD Biosciences) followed by intracellular staining for 60 minutes at 4C. Cells were washed with staining media and stained with 100 nmol/L iridium-labeled DNA-intercalator (Fluidigm) in PBS containing 0.3% saponin and 1.6% formaldehyde at 4 C for up to 48 hours. Cells were washed twice with deionized water prior to adding EQ normalization beads containing Ce140, Eu151, Eu153, Ho165, and Lu175 (Fluidigm) and acquiring on a Helios mass cytometer by The Flow and Mass Cytometry Facility, The Hospital for Sick Children. After normalizing and randomizing values near zero using the Helios software, FCS files were uploaded to Cytobank for analysis.

RNA sequencing. *Inpp4b*$^{+/+}$ or *Inpp4b*$^{-/-}$ *MLL-AF9* leukemias (3 in total for each genotype) were sorted for Venus+ before isolation of total cellular RNA with a RNeasy isolation kit (Qiagen). A Bioanalyzer 2100 (Agilent) was used for quality control and quantification. Illumina MouseRef-8 v2.0 Expression BeadChip kits were used for genome-wide expression profiling according to standard protocols at The Centre for Applied Genomics core facility at the Hospital for Sick Children. R Bioconductor 2.13.0 software was used for data processing and other statistical analyses. Raw signals from 25,697 probes

were pre-processed for background subtraction, quantile normalization and log2 transformation before the use of moderated t-tests from the Bioconductor software package Limma (linear models for microarray data). Empirical Bayes smoothing was applied to the standard errors. Paired t-tests were used for the identification of differentially expressed genes expression in each genotype subset, and the false-discovery rate (FDR) was estimated with the Benjamini-Hochberg method to correct for multiple testing. Pearson correlations showed that technical replicates had very high correlations between chips. For genes represented by multiple probe sets on the array, we selected the ones with the highest ANOVA F-statistics (lowest FDR-adjusted q value).

Gene Set Enrichment Analysis (GSEA). GSEA was performed on the datasets using GSEA v.4.0.3 provided by the Broad Institute (http://software.broadinstitute.org/gsea/downloads.jsp). Samples were rank ordered and split by *INPP4B* status, 25% high/75% low (human) or *Inpp4b*$^{+/+}$/*Inpp4b*$^{-/-}$ (mouse). Enriched gene sets were identified by 1,000 phenotype permutations in the human datasets, and 1,000 gene set permutations in the mouse dataset. Gene sets with a nominal *p*--value < 0.05 were considered significantly enriched. The curated KEGG (CP: KEGG) and BROWN_MYLEOID_CELL_DEVELOPMENT_UP gene set were obtained from MSigDB Collections (http://software.broadinstitute.org/gsea/msigdb/collections.jsp) and the LSC17 and Lysosomal Proteins gene sets were generated from the indicated publication [7,82].

Gene Network Analysis. The lysosome interacting genes were passed through String-db.v.11 [83]. and the combined binding score for each protein-protein interaction was obtained. This output, which is experimentally determined and annotated, connects the protein nodes. The absolute log fold change from the RNAseq is used to size the nodes and the colour corresponds to the -$\log_{10}$(Pvalue). The interaction map was generated by 'ForceAtlas2' in Gephi.v.0.9.2. [84].

Cells and *in vitro* cell culture. *MLL-AF9* leukemia cells were maintained in IMDM medium supplemented with 10% fetal bovine serum and cytokines: 20 ng/ml SCF, 10 ng/ml IL-6 and 10 ng/ml IL-3 (Stem Cell Technologies). OCI-AML2 cells were cultured in alpha minimal essential medium with 10% fetal bovine serum, 100□units/ml penicillin and 100□ug/ml streptomycin at 37□°C and 5% CO2. Lentiviruses were produced by calcium phosphate transfection of 293T cells with psPAX2 and VSVG as described by the manufacturer (Life Technologies, Burlington, ON, Canada). Viral particles in supernatants collected at 48 and 72□h post-transfection were enriched with Lenti-X Concentrator (Clontech, Mountain View, CA, USA). OCI-AML2 were infected with lentivirus for 24□h with 8□ug/ml protamine sulfate and selected with 2ug/mL puromycin selection. Generation of pSMAL-Puro-FLAG-INPP4B was previously described [11]. Inducible INPP4B-OCI-AML2 were generated by inserting a donor vector containing an inducible TRE3G-3xFLAG-INPP4B and constitutive Tet-On 3G expression

cassettes into the *AAVS1* safe harbor locus by CRISPR editing using an AAVS1-specific guide construct pLCKO_AAVS1_sgRNA_2, a gift from Jason Moffat (Addgene plasmid # 155085 ; http://n2t.net/addgene:155085 ; RRID:Addgene_155085). 3xFLAG-INPP4B was cloned by PCR into AscI and PacI sites of the pAAVS1-tet-iCas9-BFP2 vector, a gift from Jason Moffat (Addgene plasmid # 125519 ; http://n2t.net/addgene:125519 ; RRID:Addgene_125519). INPP4B was knocked out in constitutive Cas9 expressing OCI-AML2 cells, generated by infecting with lentiCas9-Blast [a gift from Feng Zhang (Addgene plasmid # 52962 ; http://n2t.net/addgene:52962 ; RRID:Addgene_52962)] followed by blasticidin selection. Cas9 activity was confirmed using pXPR_011 [(a gift from John Doench & David Root (Addgene plasmid # 59702 ; http://n2t.net/addgene:59702 ; RRID:Addgene_59702)]. Lentiviral INPP4B sgRNAs were generated by cloning the following sequences TTTCGCAGATTGTCCCAATG (*INPP4B*-sgRNA-1) and ACTTGTGAACTGACAGTCCC (*INPP4B*-sgRNA-2) into lentiGuide-Puro [a gift from Feng Zhang (Addgene plasmid # 52963 ; http://n2t.net/addgene:52963 ; RRID:Addgene_52963)].

Immunoblotting and Immunofluorescence. Western blotting was performed with anti-INPP4B (#8450), TFEB (#4240), HDAC2 (#2540) and b-Actin (#4967) from Cell Signaling Technology. For TFEB immunostaining OCI-AML-2 cells were centrifuged at 200xg for 10 min onto poly-L-Lysine coated slides and fixed with 4% paraformaldehyde and permeabilized with 0.1 % Triton X-100 in PBS for 10 min followed by blocking with blocking buffer (10% FBS and 5% BSA in PBS). Cells were incubated overnight at 4°C with mouse anti-human TFEB monoclonal antibody (1:50, R&D systems) in blocking buffer. Dylight-488 conjugated goat anti-mouse IgG secondary antibody (1:1000, Thermo) was added to cells in 0.025% Tween-20 in PBS for 1 h at room temperature. Nuclei were stained with 1 µg/ml DAPI and coverslips were mounted onto microscope slides with DAKO fluorescent mounting media. Cells imaged with ZEISS AxioImager M2 Epifluorescence microscope connected to AxioCam MRm CCD camera and controlled by AxioVision Software Version 4.8 at 40x 1.4 N.A. objective (Carl Zeiss, Oberkochen, Germany). Images were imported onto ImageJ. Intensity threshold applied to select DAPI positive regions and generating a mask, which was applied to green (TFEB immunostain) channel to measure TFEB intensity on DAPI positive regions. Whole cell TFEB intensity was recorded to obtain nuclear to cytosol TFEB intensity ratio.

RT-PCR. Qiagen RNeasy mini kit (Qiagen, Venlo, Netherlands) used to extract RNA from OCI-AML2 cells. Superscript IV Vilo cDNA synthesis kit (Thermo) was used to reverse transcribe equal amounts of RNA. TaqMan Fast Advanced Master mix (Applied Biosystems, Foster City, CA) and Taqman assays used to amplify cDNA through quantitative PCR according to manufacturer instructions with QuantStudio 3 Real-Time PCR system (Thermo Fisher) controlled by QuantStudio Design and AnalysisSoftware version 1.2 (Thermo Fisher). Taqman assays include Actb (Hs03023943_g1), CtsD

(Hs00924259_m1), CtsB (Hs00157194_m1), Atp6v1h (Hs00977530_m1), Atp6v1d (Hs00211133_m1), Lamp1 (Hs05049889_s1) and Mcoln1 (Hs01100661_g1) and performed in triplicates. Gene expression determined through relative quantification (ΔΔCt method) and normalized to Actb. Three biological triplicates were performed and displayed as fold increases, statistics were performed by using a students t-test where $P < 0.05$ was significant.

Luciferase Assay. HEK293T cells were cotransfected with 4X-CLEAR promoter-reporter construct [a gift from Albert La Spada (Addgene plasmid # 66800 ; http://n2t.net/addgene:66800 ; RRID:Addgene_66800)] and a CMV-promoter Renilla luciferase vector was used as the internal control with either pSMAL empty vector or pSMAL-INPP4B. Three biological triplicates were performed and displayed as fold increases, statistics were performed by using a students t-test where $P < 0.05$ was significant.

Lysosome Assays. For Lysotracker Assays the LysoTracker™ Red DND-99 (Thermo L7528) reagent was used. 0.5×10^6 OCI-AML2 cells were stained in the dark with 1mM Lysotracker in 500 mL of PBS for 15 min at 37°C. For Cathepsin B Assays, the Magic Red Cathepsin B Assay Kit (Abcam ab270772) was used as according to supplied protocol. Briefly, after preparing Magic Red reagent 1×10^6 OCI-AML2 cells in 500 mL were stained in the dark for 30 min at 37°C. After staining of cells with either reagent, cells were washed with PBS and imaging and quantitation were as follows. 1×10^5 stained cells were centrifuged at 200 xg for 10 min onto poly-L-Lysine coated coverslips were immediately mounted onto microscope slides with DAKO fluorescent and imaged with EVOS-FL fluorescent inverted microscope controlled by EVOS XL core imaging system at 20x 0.4 N.A. objective (Thermo Fisher). Remaining cells were analysed by flow cytometry with Beckman Coulter Cytoflex flow cytometer (Beckman, Brea, CO). Background signal was determined with non-labelled cells. A minimum of 10,000 gated events were counted per condition using the phycoerythrin (PE-A) channel for quantitation. For DQ-BSA experiments, OCI-AML2-Tet-ON-INPP4B cells (treated with or without doxycycline (100ng/mL) 48 h prior to lysosome labelling) or MLL-AF9 Inpp4b$^{+/+}$ and Inpp4b$^{-/-}$ cells were incubated with 10ug/mL DQ Red BSA (Invitrogen) or 2uM Alexa-647-conjugated 10kDa dextran (Invitrogen) in complete media for 1h to 6h at 37°C. At each time point, cells were washed twice with PBS and subsequently analyzed for by flow cytometry with Beckman Coulter Cytoflex flow cytometer (Beckman, Brea, CO). A total of 60,000 events were collected per sample per time point using the APC channel. Non-labeled cells were used as control for determining background signal and as time point 0. At least three biological triplicates were performed and displayed as relative fluorescence intensity, statistics were performed by using a paired students t-test where $P < 0.05$ was significant.

Quantification and Statistical Analysis.

Errors bars show standard error of the mean (SEM). Data were analyzed with a two-tailed Student t-test for comparison of the means of two groups and by one-way ANOVA unless otherwise stated. *P* values of less than 0.05 were considered statistically significant. No randomization of mice or 'blinding' of researchers to sample identity was used during the analyses. Sample sizes were not predetermined on the basis of expected effect size, but rough estimations were made on the basis of pilot experiments and measurements. No data exclusion was applied.

References

1. Papaemmanuil, E. *et al.* Genomic classification and prognosis in acute myeloid leukemia. *N. Engl. J. Med.* **374,** 2209–2221 (2016).
2. Siegel, R. L., Miller, K. D. & Jemal, A. Cancer statistics, 2018. *CA Cancer J Clin* **68,** 7–30 (2018).
3. Dick, J. E. Stem cell concepts renew cancer research. *Blood* **112,** 4793–4807 (2008).
4. Kreso, A. & Dick, J. E. Evolution of the cancer stem cell model. *Cell Stem Cell* **14,** 275–291 (2014).
5. Eppert, K. *et al.* Stem cell gene expression programs influence clinical outcome in human leukemia. *Nat. Med.* **17,** 1086–1093 (2011).
6. van Rhenen, A. *et al.* High stem cell frequency in acute myeloid leukemia at diagnosis predicts high minimal residual disease and poor survival. *Clin. Cancer Res.* **11,** 6520–6527 (2005).
7. Ng, S. W. K. *et al.* A 17-gene stemness score for rapid determination of risk in acute leukaemia. *Nature* **540,** 433–437 (2016).
8. Shlush, L. I. *et al.* Tracing the origins of relapse in acute myeloid leukaemia to stem cells. *Nature* **547,** 104–108 (2017).
9. Fransecky, L., Mochmann, L. H. & Baldus, C. D. Outlook on PI3K/AKT/mTOR inhibition in acute leukemia. *Mol. Cell. Ther.* **3,** 2 (2015).
10. Kandoth, C. *et al.* Mutational landscape and significance across 12 major cancer types. *Nature* **502,** 333–339 (2013).
11. Dzneladze, I. *et al.* INPP4B overexpression is associated with poor clinical outcome and therapy resistance in acute myeloid leukemia. *Leukemia* **29,** 1485–1495 (2015).
12. Norris, F. A., Auethavekiat, V. & Majerus, P. W. The isolation and characterization of cDNA encoding human and rat brain inositol polyphosphate 4-phosphatase. *J. Biol. Chem.* **270,** 16128–16133 (1995).
13. Norris, F. A., Atkins, R. C. & Majerus, P. W. The cDNA cloning and characterization of inositol polyphosphate 4-phosphatase type II. Evidence for conserved alternative splicing in the 4-phosphatase family. *J. Biol. Chem.* **272,** 23859–23864 (1997).
14. Franke, T. F., Kaplan, D. R., Cantley, L. C. & Toker, A. Direct regulation of the Akt proto-oncogene product by phosphatidylinositol-3,4-bisphosphate. *Science* **275,** 665–668 (1997).
15. Frech, M. *et al.* High affinity binding of inositol phosphates and phosphoinositides to the pleckstrin homology domain of RAC/protein kinase B and their influence on kinase activity. *J. Biol. Chem.* **272,** 8474–8481 (1997).
16. Scheid, M. P. *et al.* Phosphatidylinositol (3,4,5)P3 is essential but not sufficient for protein kinase B (PKB) activation; phosphatidylinositol (3,4)P2 is required for PKB phosphorylation at Ser-473: studies using cells from SH2-containing inositol-5-phosphatase knockout mice. *J. Biol. Chem.* **277,** 9027–9035 (2002).
17. Hodgson, M. C. *et al.* Decreased expression and androgen regulation of the tumor suppressor gene INPP4B in prostate cancer. *Cancer Res.* **71,** 572–582 (2011).
18. Cancer Genome Atlas Network. Comprehensive molecular portraits of human breast tumours. *Nature* **490,** 61–70 (2012).
19. Fedele, C. G. *et al.* Inositol polyphosphate 4-phosphatase II regulates PI3K/Akt signaling and is lost in human basal-like breast cancers. *Proc. Natl. Acad. Sci. USA* **107,** 22231–22236 (2010).
20. Gewinner, C. *et al.* Evidence that inositol polyphosphate 4-phosphatase type II is a tumor suppressor that inhibits PI3K signaling. *Cancer Cell* **16,** 115–125 (2009).

21. Hodgson, M. C. *et al.* INPP4B suppresses prostate cancer cell invasion. *Cell Commun. Signal.* **12,** 61 (2014).
22. Recher, C. INPP4B, a new player in the chemoresistance of AML. *Blood* **125,** 2738–2739 (2015).
23. Rijal, S. *et al.* Inositol polyphosphate 4-phosphatase II (INPP4B) is associated with chemoresistance and poor outcome in AML. *Blood* **125,** 2815–2824 (2015).
24. Wang, P. *et al.* INPP4B-mediated DNA repair pathway confers resistance to chemotherapy in acute myeloid leukemia. *Tumour Biol.* **37,** 12513–12523 (2016).
25. Zhang, F., Zhu, J., Li, J., Zhu, F. & Zhang, P. IRF2-INPP4B axis participates in the development of acute myeloid leukemia by regulating cell growth and survival. *Gene* **627,** 9–14 (2017).
26. Gasser, J. A. *et al.* SGK3 mediates INPP4B-dependent PI3K signaling in breast cancer. *Mol. Cell* **56,** 595–607 (2014).
27. Guo, S. T. *et al.* INPP4B is an oncogenic regulator in human colon cancer. *Oncogene* **35,** 3049–3061 (2016).
28. Chi, M. N. *et al.* INPP4B is upregulated and functions as an oncogenic driver through SGK3 in a subset of melanomas. *Oncotarget* **6,** 39891–39907 (2015).
29. Rodgers, S. J. *et al.* INPP4B promotes PI3Kα-dependent late endosome formation and Wnt/β-catenin signaling in breast cancer. *Nat. Commun.* **12,** 3140 (2021).
30. Dzneladze, I. *et al.* SubID, a non-median dichotomization tool for heterogeneous populations, reveals the pan-cancer significance of INPP4B and its regulation by EVI1 in AML. *PLoS One* **13,** e0191510 (2018).
31. Cancer Genome Atlas Research Network *et al.* Genomic and epigenomic landscapes of adult de novo acute myeloid leukemia. *N. Engl. J. Med.* **368,** 2059–2074 (2013).
32. Verhaak, R. G. W. *et al.* Prediction of molecular subtypes in acute myeloid leukemia based on gene expression profiling. *Haematologica* **94,** 131–134 (2009).
33. Metzeler, K. H. *et al.* An 86-probe-set gene-expression signature predicts survival in cytogenetically normal acute myeloid leukemia. *Blood* **112,** 4193–4201 (2008).
34. Balgobind, B. V. *et al.* Evaluation of gene expression signatures predictive of cytogenetic and molecular subtypes of pediatric acute myeloid leukemia. *Haematologica* **96,** 221–230 (2011).
35. Klein, H.-U. *et al.* Quantitative comparison of microarray experiments with published leukemia related gene expression signatures. *BMC Bioinformatics* **10,** 422 (2009).
36. Jung, N., Dai, B., Gentles, A. J., Majeti, R. & Feinberg, A. P. An LSC epigenetic signature is largely mutation independent and implicates the HOXA cluster in AML pathogenesis. *Nat. Commun.* **6,** 8489 (2015).
37. Laurenti, E. *et al.* CDK6 levels regulate quiescence exit in human hematopoietic stem cells. *Cell Stem Cell* **16,** 302–313 (2015).
38. Laurenti, E. *et al.* The transcriptional architecture of early human hematopoiesis identifies multilevel control of lymphoid commitment. *Nat. Immunol.* **14,** 756–763 (2013).
39. Lechman, E. R. *et al.* miR-126 Regulates Distinct Self-Renewal Outcomes in Normal and Malignant Hematopoietic Stem Cells. *Cancer Cell* **29,** 214–228 (2016).
40. Notta, F. *et al.* Distinct routes of lineage development reshape the human blood hierarchy across ontogeny. *Science* **351,** aab2116 (2016).
41. Novershtern, N. *et al.* Densely interconnected transcriptional circuits control cell states in human hematopoiesis. *Cell* **144,** 296–309 (2011).
42. Rapin, N. *et al.* Comparing cancer vs normal gene expression profiles identifies new disease entities and common transcriptional programs in AML patients. *Blood* **123,** 894–904 (2014).
43. Lara-Astiaso, D. *et al.* Immunogenetics. Chromatin state dynamics during blood formation. *Science* **345,** 943–949 (2014).
44. Pietras, E. M. *et al.* Functionally Distinct Subsets of Lineage-Biased Multipotent Progenitors Control Blood Production in Normal and Regenerative Conditions. *Cell Stem Cell* **17,** 35–46 (2015).
45. Ferron, M. *et al.* Inositol polyphosphate 4-phosphatase B as a regulator of bone mass in mice and humans. *Cell Metab.* **14,** 466–477 (2011).
46. Kofuji, S. *et al.* INPP4B is a ptdins(3,4,5)p3 phosphatase that can act as a tumor suppressor. *Cancer Discov.* **5,** 730–739 (2015).

47. Li Chew, C. *et al.* In Vivo Role of INPP4B in Tumor and Metastasis Suppression through Regulation of PI3K-AKT Signaling at Endosomes. *Cancer Discov.* **5,** 740–751 (2015).
48. Somervaille, T. C. P. & Cleary, M. L. Identification and characterization of leukemia stem cells in murine MLL-AF9 acute myeloid leukemia. *Cancer Cell* **10,** 257–268 (2006).
49. Sardiello, M. *et al.* A gene network regulating lysosomal biogenesis and function. *Science* **325,** 473–477 (2009).
50. Rouillard, A. D. *et al.* The harmonizome: a collection of processed datasets gathered to serve and mine knowledge about genes and proteins. *Database (Oxford)* **2016,** (2016).
51. Mandegar, M. A. *et al.* CRISPR Interference Efficiently Induces Specific and Reversible Gene Silencing in Human iPSCs. *Cell Stem Cell* **18,** 541–553 (2016).
52. Marwaha, R. & Sharma, M. DQ-Red BSA Trafficking Assay in Cultured Cells to Assess Cargo Delivery to Lysosomes. *Bio Protoc* **7,** (2017).
53. Amaravadi, R. K. & Winkler, J. D. Lys05: a new lysosomal autophagy inhibitor. *Autophagy* **8,** 1383–1384 (2012).
54. Cechakova, L. *et al.* A potent autophagy inhibitor (lys05) enhances the impact of ionizing radiation on human lung cancer cells H1299. *Int. J. Mol. Sci.* **20,** (2019).
55. McAfee, Q. *et al.* Autophagy inhibitor Lys05 has single-agent antitumor activity and reproduces the phenotype of a genetic autophagy deficiency. *Proc. Natl. Acad. Sci. USA* **109,** 8253–8258 (2012).
56. Jin, H. *et al.* INPP4B promotes cell survival via SGK3 activation in NPM1-mutated leukemia. *J Exp Clin Cancer Res* **37,** 8 (2018).
57. Zhang, F. *et al.* IRF2-INPP4B-mediated autophagy suppresses apoptosis in acute myeloid leukemia cells. *Biol. Res.* **52,** 11 (2019).
58. Zhang, F. *et al.* IRF2-INPP4B axis inhibits apoptosis of acute myeloid leukaemia cells via regulating T helper 1/2 cell differentiation. *Cell Biochem. Funct.* **38,** 582–590 (2020).
59. Luzio, J. P. *et al.* Lysosome-endosome fusion and lysosome biogenesis. *J. Cell Sci.* **113 (Pt 9),** 1515–1524 (2000).
60. Settembre, C. & Ballabio, A. Lysosome: regulator of lipid degradation pathways. *Trends Cell Biol.* **24,** 743–750 (2014).
61. Lawrence, R. E. & Zoncu, R. The lysosome as a cellular centre for signalling, metabolism and quality control. *Nat. Cell Biol.* **21,** 133–142 (2019).
62. Savini, M., Zhao, Q. & Wang, M. C. Lysosomes: signaling hubs for metabolic sensing and longevity. *Trends Cell Biol.* **29,** 876–887 (2019).
63. Lamming, D. W. & Bar-Peled, L. Lysosome: The metabolic signaling hub. *Traffic* **20,** 27–38 (2019).
64. Inpanathan, S. & Botelho, R. J. The lysosome signaling platform: adapting with the times. *Front. Cell Dev. Biol.* **7,** 113 (2019).
65. Leeman, D. S. *et al.* Lysosome activation clears aggregates and enhances quiescent neural stem cell activation during aging. *Science* **359,** 1277–1283 (2018).
66. Liang, R. *et al.* Restraining lysosomal activity preserves hematopoietic stem cell quiescence and potency. *Cell Stem Cell* **26,** 359–376.e7 (2020).
67. Loeffler, D. *et al.* Publisher Correction: Asymmetric lysosome inheritance predicts activation of haematopoietic stem cells. *Nature* **573,** E5 (2019).
68. García-Prat, L. *et al.* TFEB-mediated endolysosomal activity controls human hematopoietic stem cell fate. *Cell Stem Cell* **28,** 1838–1850.e10 (2021).
69. Sukhai, M. A. *et al.* Lysosomal disruption preferentially targets acute myeloid leukemia cells and progenitors. *J. Clin. Invest.* **123,** 315–328 (2013).
70. Bernard, D. *et al.* Select microtubule inhibitors increase lysosome acidity and promote lysosomal disruption in acute myeloid leukemia (AML) cells. *Apoptosis* **20,** 948–959 (2015).
71. Yun, S. *et al.* TFEB links MYC signaling to epigenetic control of myeloid differentiation and acute myeloid leukemia. *Blood Cancer Discov.* **2,** 162–185 (2021).
72. Frenquelli, M. & Tonon, G. WNT signaling in hematological malignancies. *Front. Oncol.* **10,** 615190 (2020).
73. Grainger, S., Traver, D. & Willert, K. Wnt signaling in hematological malignancies. *Prog Mol Biol Transl Sci* **153,** 321–341 (2018).
74. Rafiq, S., McKenna, S. L., Muller, S., Tschan, M. P. & Humbert, M. Lysosomes in acute myeloid

leukemia: potential therapeutic targets? *Leukemia* **35,** 2759–2770 (2021).
75. Hanahan, D. Hallmarks of cancer: new dimensions. *Cancer Discov.* **12,** 31–46 (2022).
76. Zhitomirsky, B. & Assaraf, Y. G. Lysosomes as mediators of drug resistance in cancer. *Drug Resist Updat* **24,** 23–33 (2016).
77. Huang, D. W., Sherman, B. T. & Lempicki, R. A. Systematic and integrative analysis of large gene lists using DAVID bioinformatics resources. *Nat. Protoc.* **4,** 44–57 (2009).
78. Huang, D. W., Sherman, B. T. & Lempicki, R. A. Bioinformatics enrichment tools: paths toward the comprehensive functional analysis of large gene lists. *Nucleic Acids Res.* **37,** 1–13 (2009).
79. Gu, Z., Gu, L., Eils, R., Schlesner, M. & Brors, B. circlize Implements and enhances circular visualization in R. *Bioinformatics* **30,** 2811–2812 (2014).
80. Zuber, J. *et al.* Mouse models of human AML accurately predict chemotherapy response. *Genes Dev.* **23,** 877–889 (2009).
81. Hu, Y. & Smyth, G. K. ELDA: extreme limiting dilution analysis for comparing depleted and enriched populations in stem cell and other assays. *J. Immunol. Methods* **347,** 70–78 (2009).
82. Palmieri, M. *et al.* Characterization of the CLEAR network reveals an integrated control of cellular clearance pathways. *Hum. Mol. Genet.* **20,** 3852–3866 (2011).
83. Szklarczyk, D. *et al.* STRING v11: protein-protein association networks with increased coverage, supporting functional discovery in genome-wide experimental datasets. *Nucleic Acids Res.* **47,** D607–D613 (2019).
84. Jacomy, M., Venturini, T., Heymann, S. & Bastian, M. ForceAtlas2, a continuous graph layout algorithm for handy network visualization designed for the Gephi software. *PLoS One* **9,** e98679 (2014).
85. Herold, T. *et al.* A 29-gene and cytogenetic score for the prediction of resistance to induction treatment in acute myeloid leukemia. *Haematologica* **103,** 456–465 (2018).
86. Wouters, B. J. *et al.* Double CEBPA mutations, but not single CEBPA mutations, define a subgroup of acute myeloid leukemia with a distinctive gene expression profile that is uniquely associated with a favorable outcome. *Blood* **113,** 3088–3091 (2009).
87. Valk, P. J. M. *et al.* Prognostically useful gene-expression profiles in acute myeloid leukemia. *N. Engl. J. Med.* **350,** 1617–1628 (2004).

Supplementary Figure Information

Supplementary Figure 1. A. Heatmaps of LSC-17 gene expression in AML patient datasets, ranked by INPP4B expression (INPP4B-high quartile highlighted dark blue). **B.** Gene set enrichment analysis (GSEA) enrichment plot of the LSC-17 gene set in the Wouters, Klein, TCGA, Herold and Metzeler AML patient datasets ranked by *INPP4B* AML expression. **C.** Relative expression of *INPP4B* in sorted human or (**D)** sorted mouse hematopoietic stem and progenitor cells.

Supplementary Figure 2. A. Total bone marrow cellularity from age- and sex-matched *Inpp4b*$^{+/+}$ and *Inpp4B*$^{-/-}$ mice (*n*=10, ±S.E.M.). **B.** Total peripheral blood counts from age- and sex-matched adult *Inpp4b*$^{+/+}$ and *Inpp4b*$^{-/-}$ mice (normalized to control. *n*=10, mean ± SEM). **C.** Flow cytometry gating strategy for immunophenotyping of HSPCs in *Inpp4b*$^{+/+}$ and *Inpp4B*$^{-/-}$ mice. **D.** Representative contour plot of EPCR expression in *Inpp4b*$^{+/+}$ and *Inpp4B*$^{-/-}$ LT-HSCs. **E.** Individual colony counts separated by colony type from weekly serial replating of total bone marrow from age- and sex-matched *Inpp4b*$^{+/+}$ and *Inpp4B*$^{-/-}$ mice (*n*=6, ±S.E.M.). **F.** Flow cytometry gating strategy for CD45.2 (test cells) and CD45.1

(competitor cells) percentages in myeloid cells in long term competitive transplant assays. **G.** Relative contribution of *Inpp4b*$^{+/+}$, *Inpp4b*$^{+/-}$ and *Inpp4b*$^{-/-}$ long term HSCs to the regeneration of the total and myeloid CD45.1 (competitor) and CD45.2 (donor) populations in competitive transplant experiments at 20 weeks and 64 weeks (*n*=10, ±S.E.M.)

Supplementary Figure 3. A. Gating strategy for generation of *MLL-AF9* murine leukemias from age- and sex-matched adult *Inpp4b*$^{+/+}$ and *Inpp4b*$^{-/-}$ mice, expressing both Gr-1 and Mac-1 surface markers. **B.** Scatter plots of % positive cell surface markers shown. T-test performed with Welch's correction. **C**. Scatter plots of median intensity of cell surface markers shown. T-test performed with Welch's correction.

Supplementary Figure 4. A. Scatter plot of TPM (transcript per million) values from genes with significantly altered expression in Inpp*4b*$^{+/+}$ and *Inpp4b*$^{-/-}$ *MLL-AF9* leukemia blast cells (*n* = 3 *vs*. 3, FDR < 0.01). **B.** Volcano plot of all genes from Inpp*4b*$^{+/+}$ and *Inpp4b*$^{-/-}$ *MLL-AF9* leukemia blast cells (*n* = 3 *vs*. 3, FDR < 0.01). GSEA enrichment plots demonstrating relationship between differentially expressed geneds in Inpp*4b*$^{+/+}$ and *Inpp4b*$^{-/-}$ *MLL-AF9* leukemia blast cells and (**C**) LSC17 signature, (**D**) KEGG_myeloid cell development genes (**E**) and KEGG_osteoclast differentiation genes.

Supplementary Figure 5. Histograms of the top 20 enriched KEGG gene sets in *INPP4B*-low patients from the (**A)** Herold, (**B)** Klein patient datasets ranked by normalized enrichment score (NES).

Supplementary Figure 6. A. Western blot of OCI-AML2 cells' cytosolic and nuclear extracts. **B.** OCI-AML2 INPP4B overexpressing and (**C**) knockout cells. Steady state control, FCS starved or starved and FCS fed cells were immunostained for TFEB and counterstained with DAPI.

Supplementary Figure 7. INPP4B regulates lysosomal biology in leukemia cells. A. Inducible-INPP4B OCI-AML2 cells were treated without or with doxycycline (100mg/mL) and incubated with DQ-BSA-Green™ or Dextran-Red. Fluorescence was monitored by flow cytometry hourly, for up to 6 hours. Full time course displayed. **B.** *Inpp4b*$^{+/+}$ and *Inpp4B*$^{-/-}$ *MLL-AF9* leukemia blasts were incubated with and incubated with DQ-BSA-Green™ or Dextran-Red. Fluorescence was monitored by flow cytometry hourly, for up to 8 hours. Full time course displayed. **C.** Lys05 Dose response in Inpp*4b*$^{+/+}$ and *Inpp4B*$^{-/-}$ *MLL-AF9* leukemia blasts.

Supplementary Table Information

Supplementary Table 1. Table of significantly overrepresented gene ontologies associated with the top 200 genes enriched in high *INPP4B* patient samples across several AML patient databases.

Supplementary Table 2. Differentially upregulated and downregulated genes associated with leukemia and differentiation for *Inpp4b*$^{+/+}$ and *Inpp4b*$^{-/-}$ *MLL-AF9* leukemias

Supplementary Table 3. Ranked list of biological processes most significantly influenced by *Inpp4b* deficiency as determined by Gene Set Enrichment Analysis (GSEA) using significantly altered transcripts and identified changes in key pathways.

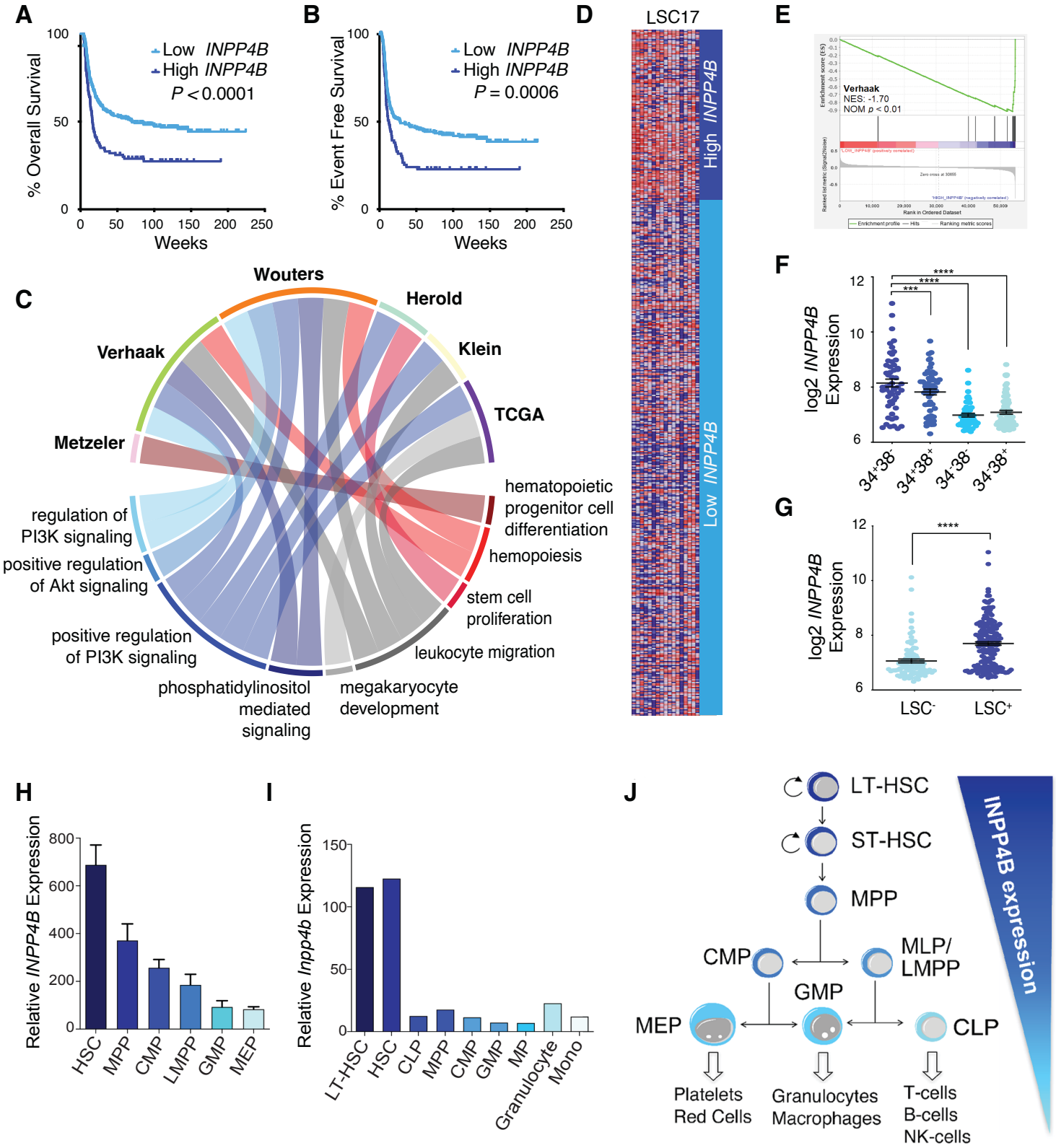

Figure 1. High levels INPP4B expression are associated with stemness signatures in leukemia and hematopoietic progenitor cells. A. Kaplan Meier analysis of overall survival in INPP4Bhigh vs. INPP4Blow AML patients from Verhaak dataset. B. Kaplan Meier analysis of event free survival in INPP4B^{high} vs. INPP4B^{low} AML patients from Verhaak dataset. C. Enriched terms related to phosphatidylinositol signaling or the hematopoietic compartment stem cells were highlighted in a chord diagram that was generated with the circlize R package (24930139). D. Heatmaps of LSC-17 gene expression in the Verhaak AML patient dataset, ranked by INPP4B expression (INPP4B-high quartile highlighted dark blue). E. Gene set enrichment analysis (GSEA) enrichment plot of the LSC-17 gene set in the Verhaak AML patient dataset ranked by INPP4B AML expression. F. Expression of INPP4B from 227 AML patient-derived samples sorted based on the expression of combinations of CD34 and CD38 surface markers. G. INPP4B expression in 278 sorted fractions characterized as LSC+ and LSC- enriched by their engraftment potential into NOD/SCID mice. H. Relative expression of INPP4B in human hematopoietic stem and progenitor cells. I. Relative expression of Inpp4b in murine hematopoietic stem and progenitor cells. J. Schematic depicting INPP4B expression in the haematopoietic hierarchy (high = dark blue, low = light blue).

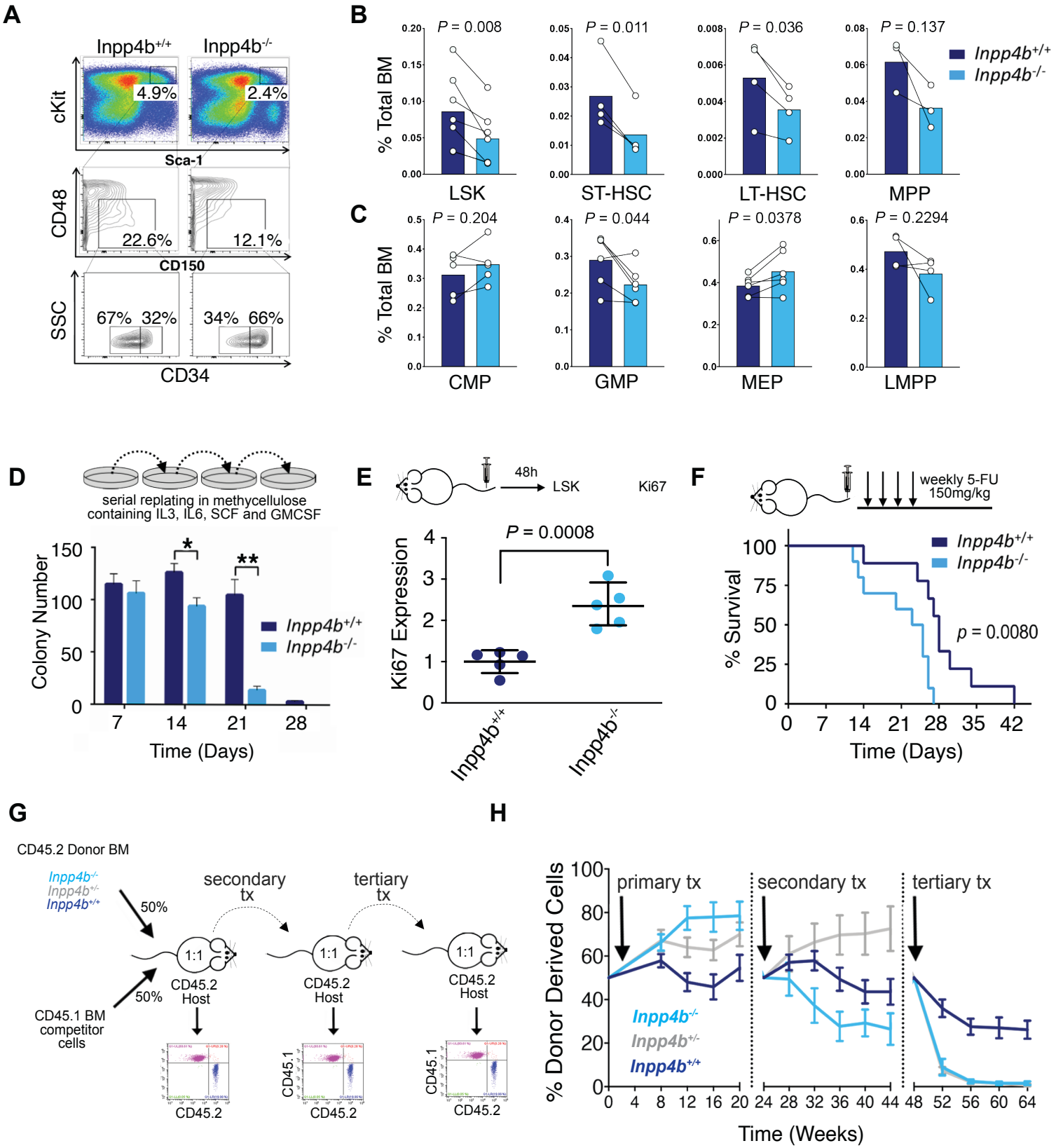

Figure 2. Inpp4b-deficiency reduces repopulation capacity of hematopoietic progenitors. A. Representative pseudocolour dot-plot and contour plot from immunophenotyping of the adult bone marrow niche in Inpp4b+/+ and Inpp4b-/- mice. B. Bone marrow stem cell fractions and (C) bone marrow progenitor fractions from age- and sex-matched adult Inpp4b+/+ and Inpp4b-/- mice, shown as a percentage of total bone marrow monocuclear cells. D. Total colony counts from weekly serial replating of total bone marrow from age- and sex-matched Inpp4b+/+ and Inpp4B-/- mice (n=6, ± S.E.M.). E. Cell cycle analysis in sorted LSK cells, 48 hours after acute myeloablation with single 5'-fluorouracil treatment, measured by intracellular Ki67 level and flow cytometry (n=5, ± S.E.M.). F. Kaplan-Meier survival analysis after serial myeloablation (5'-fluorouracil, weekly i.p.) of age- and sex-matched Inpp4b+/+ and Inpp4b-/- mice (n=10). G. Schematic describing competitive transplant experiments. H. Relative contribution of Inpp4b+/+, Inpp4b+/- and Inpp4b-/- long term HSCs to the regeneration of the myeloid populations in three consecutive competitive transplant experiments (n=10, ±S.E.M.).

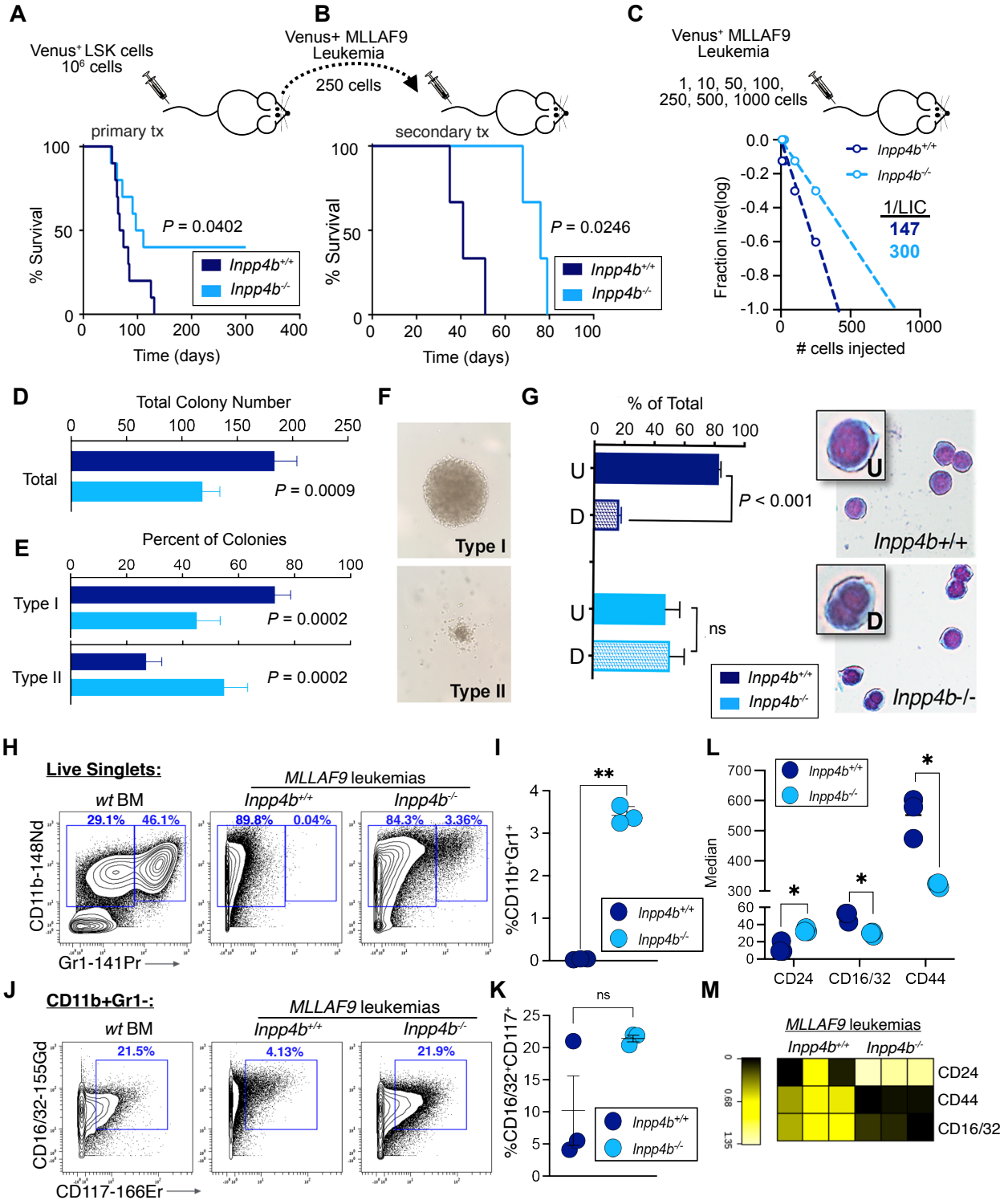

Figure 3. Inpp4b-deficient MLL-AF9 cells have a decreased leukemogenic potential and have a more differentiated phenotype. A. Kaplan-meier survival analysis of primary Venus+-MLL-AF9 leukemias generated from Inpp4b+/+ and Inpp4b-/- mouse LSK cells (n=10). B. Kaplan-meier survival analysis of secondary MLL-AF9 leukemias generated by transplantation of cells from Inpp4b+/+ and Inpp4b-/- MLL-AF9 leukemia blasts (n=6). C. Limiting dilution assay (LDA) of Inpp4b+/+ (dark blue (n=12)) and Inpp4b-/- MLL-AF9 (light blue (n=12)) leukemia cells (1000, 250, 100, and 25 cells) into host wildtype C57BL/6 mice. D. Total and percentage colony counts in LFC assays from Inpp4b+/+ and Inpp4B-/- murine MLL-AF9 leukemia blasts (n=8, ±S.E.M.). E Proportion of undifferentiated and differentiated leukemic blasts from Inpp4b+/+ (n=8, ±S.E.M.). F. Representative image of type-I and type-II colonies from secondary MLL-AF9 leukemia cells. G. Representative images of Wright–Giemsa staining of leukemic blasts from Inpp4b+/+ and Inpp4b-/- MLL-AF9 terminal leukemias; (U) undifferentiated and (D) differentiated (n=3, ±S.E.M.; left). H,I. Contour plots (10% probability) show CD11b versus Gr1 expression on live singlets from Inpp4b+/+ versus Inpp4b-/- MLL-AF9 leukemia samples compared to WT BM cells (representative of n=3/group). Scatter graph shows the % CD11b+ Gr1+ cells in each AML type. Two-tailed t-test with Welch's correction, P = 0.001. J,K. Contour plots show CD16/32 versus CD117 expression on CD11b+ Gr1- cells from representative Inpp4b+/+ and Inpp4b-/- MLL-AF9 leukemia samples. Scatter graph shows the % CD16/32+ CD117+ cells in each type of AML. Two-tailed t-test with Welch's correction, P = 0.1726. L. Multiple unpaired t-tests with Welch's correction. Multiple comparisons corrected by False Discovery Rate using the 2-stage step-up method of Benjamini, Krieger and Yekiuteli. *, Q=0.03 for each comparison shown. M. Heatmap visualization of the median metal intensity (MMI) of the indicated markers on CD11b+ Gr1- cells from each type of AML. Values for each marker were calculated as arcinsh (MMI(x)/ scale_argument)- arcsinh (control /scale_argument) where x is the sample value, control is the lowest value for the marker across all samples, and scale argument=5.

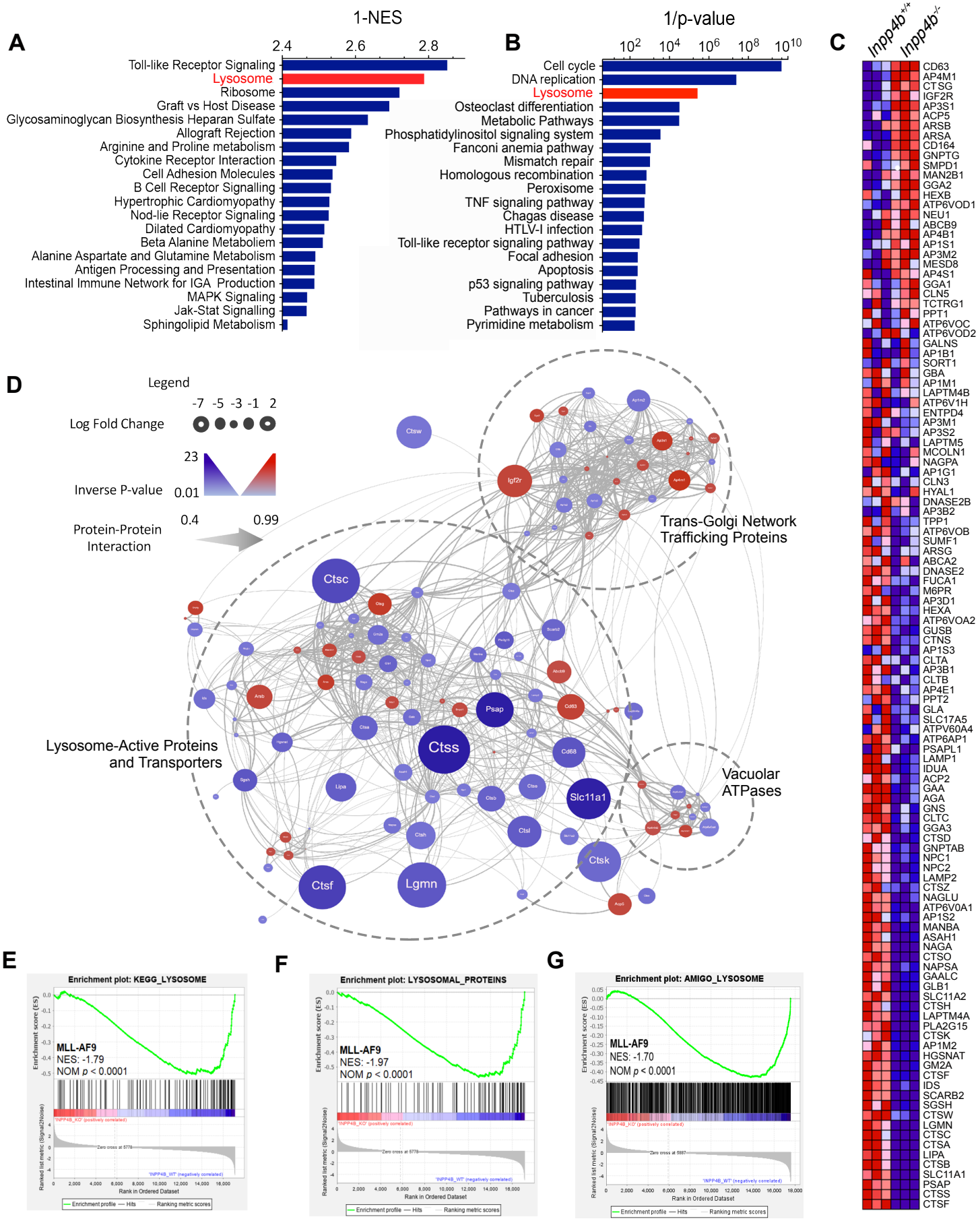

Figure 4. Inpp4b expression is associated with lysosomal gene sets. A. Top 20 enriched KEGG gene sets in Inpp4b+/+ and Inpp4b-/- MLL-AF9 leukemia blast cells determined using GSEA. B. Top 20 enriched KEGG pathways from significantly upregulated genes (log-fold-change > 1, FDR < 0.05) in Inpp4b-/- MLL-AF9 leukemia blast cells were determined using the DAVID analysis tool. C. Heat map of differentially expressed KEGG Lysosome genes from Inpp4b+/+ and Inpp4b-/- MLL-AF9 leukemia blast cells (upregulated in red, downregulated in blue). D. STRING-db analysis of differential expression of KEGG Lysosome genes from Inpp4b+/+ and Inpp4b-/- MLL-AF9 leukemia blast cells. E. Gene set expression analysis (GSEA) for Lysosome pathway genes in Inpp4b-/- MLL-AF9 leukemia blast cells witt the KEGG Lysosome gene set; (F) Lysosomal proteins gene set; (G) Harmonizome (Amigo) lysosome gene set.

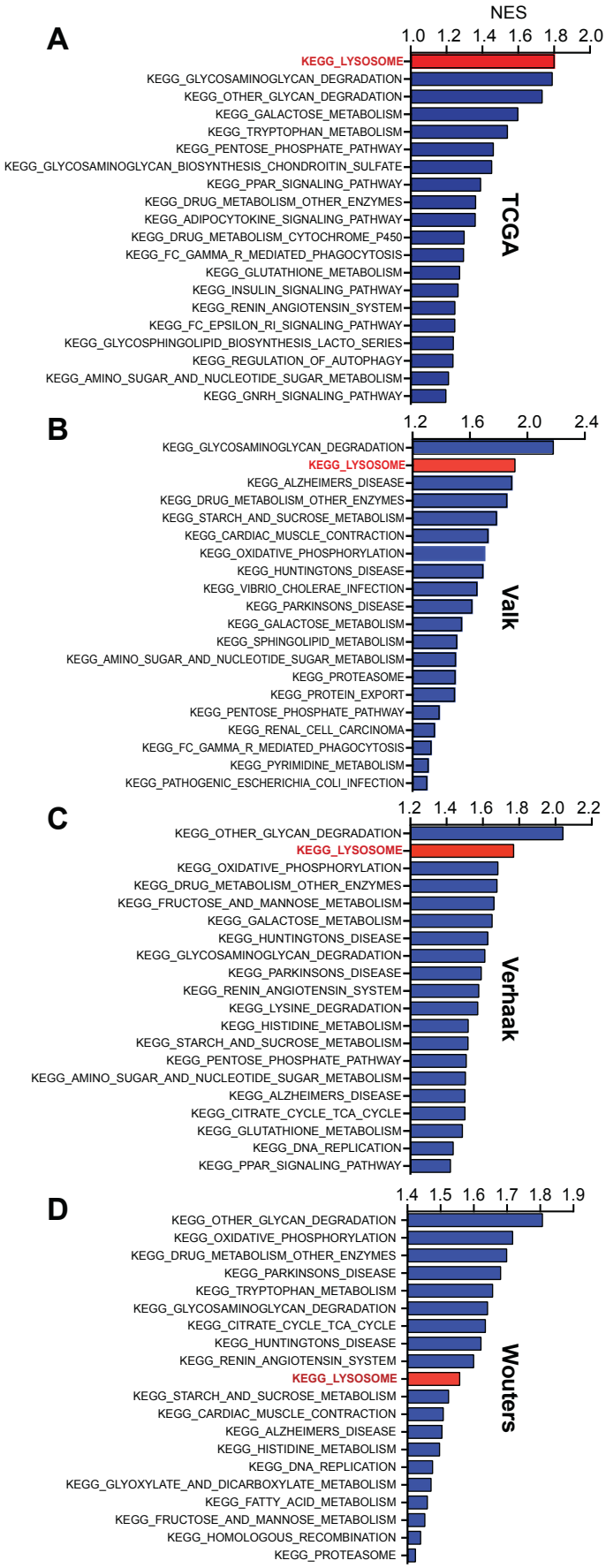

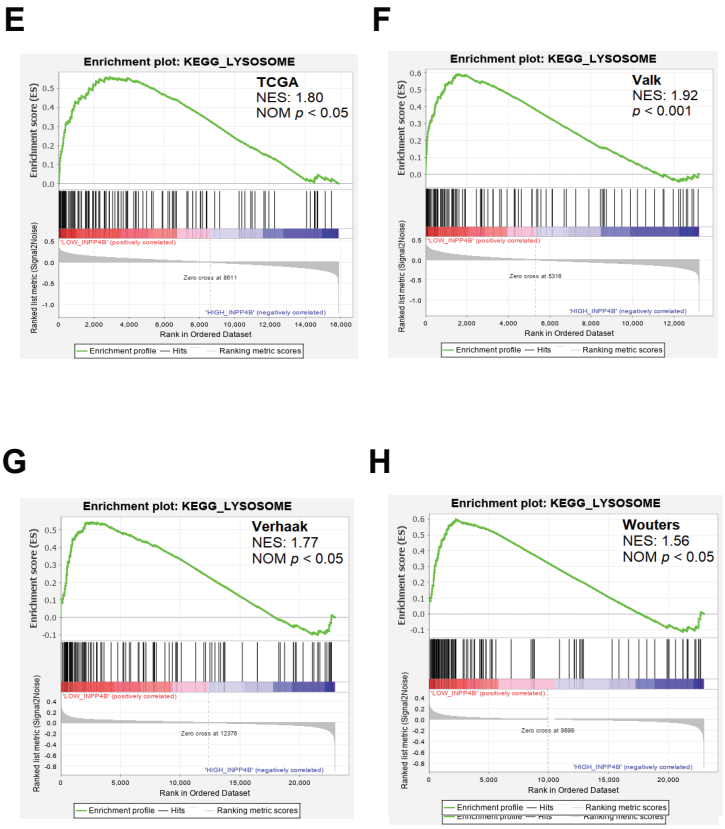

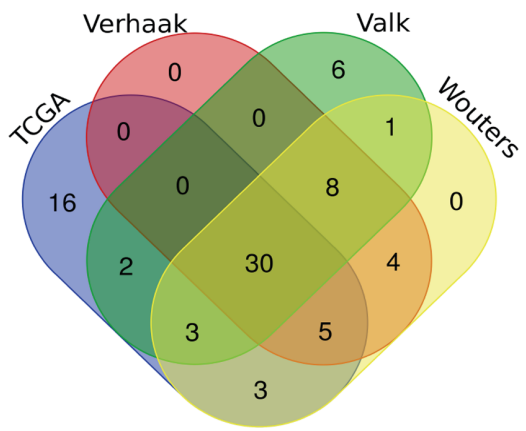

J

Core Leading Edge KEGG Lysosomal Genes				
IDUA	GM2A	AGA	CTSD	HEXB
CTSH	CTSZ	GGA2	GALNS	NPC2
SLC11a1	NAGPA	AP1s2	CD63	CTSA
LAMP1	CTSG	ATP6V0D1	TPP1	AP4M1
CLTCL1	GLA	GNS	MANBA	GAA
GUSb	ARSB	CTSB	ATP6V0B	PSAP

Figure 5: A Lysosome gene set is enriched in patients with low levels of INPP4B. Histograms of the top 20 enriched KEGG gene sets in INPP4B-low patients from the (A) TCGA, (B) Valk (C) Verhaak and (D) Wouters AML patient datasets ranked by normalized enrichment score (NES). GSEA enrichment plots of KEGG Lysosome geneset demonstrating significant enrichment with INPP4B expression in (E) TCGA, (F) Valk (G) Verhaak and (H) Wouters AML patient datasets. I. Venn diagram illustrating the number of genes from the KEGG lysosome gene set that contribute to the leading-edge subset in the four AML datasets. J. Table of the 30 common core enriched lysosome genes among the four AML datasets.

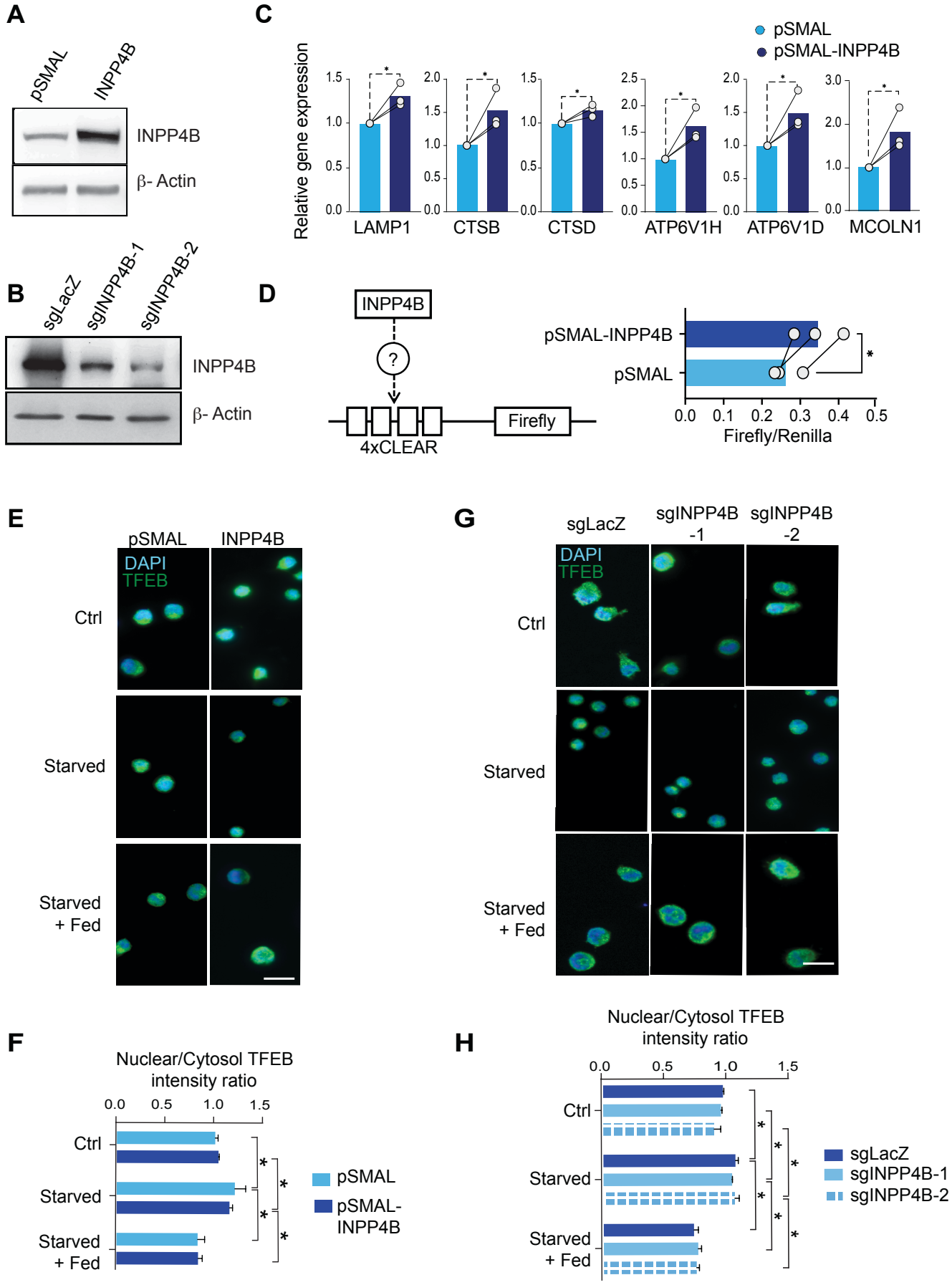

Figure 6: INPP4B promotes expression of lysosomal genes. Representative Western blots demonstrating (A) overexpression and (B) knockdown of INPP4B protein levels in OCI-AML2 cells. C. qRT-PCR analysis of lysosome gene expression in OCI-AML2 cells normalized against Actb. Shown is mean + SEM from three independent experiments. D. HEK293T cells overexpressing control or INPP4B constructs were co-transfected with pGL3 4X-CLEAR-Firefly reporter and CMV-promoter Renilla luciferase internal control and quantitated as the ratio of Firefly to Renilla. E,G. OCI-AML2 cells in the steady state, FCS starved, or starved and FCS fed conditions were immunostained for TFEB and (F,H) analyzed for nuclear/cytosol TFEB intensity.

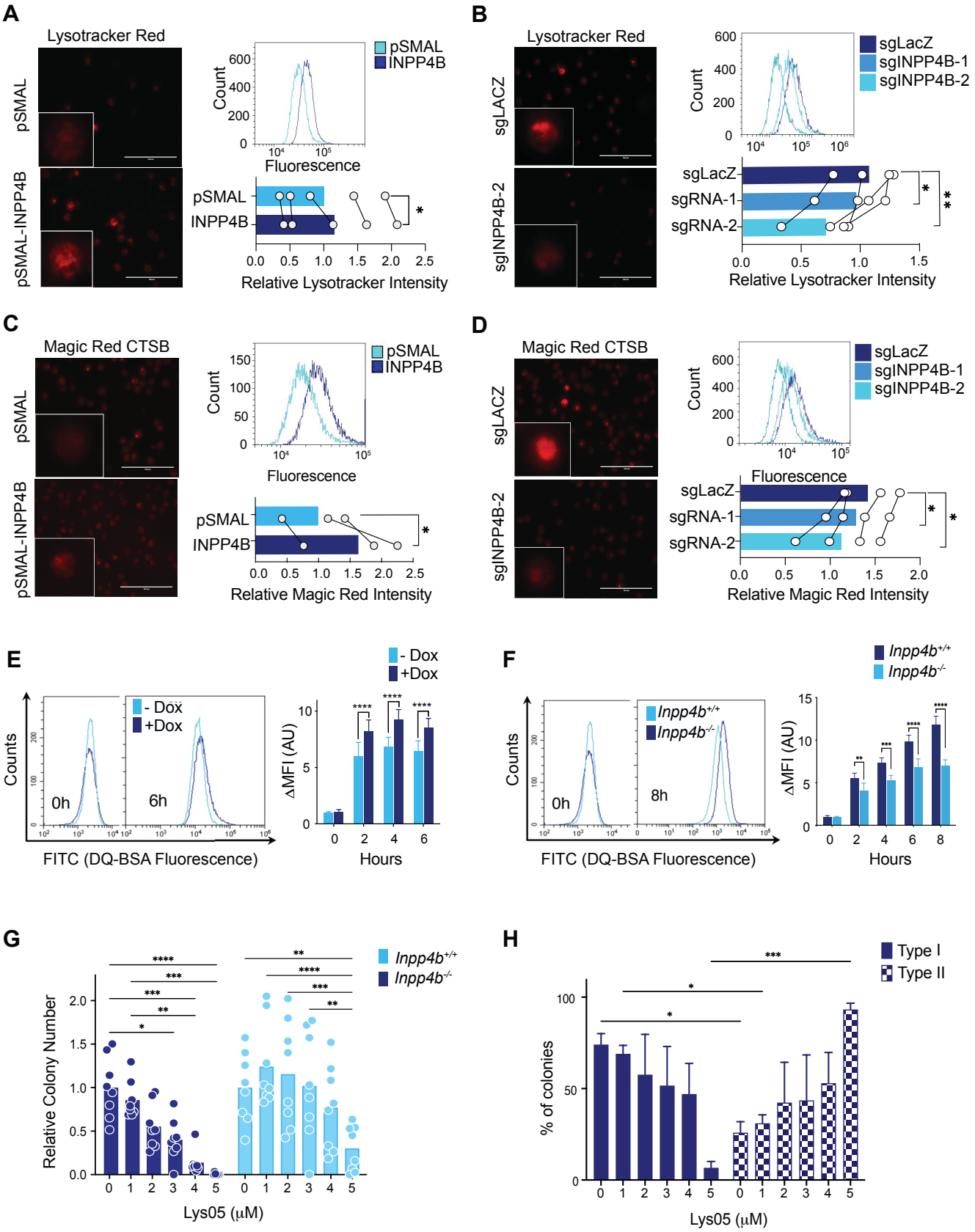

Figure 7: INPP4B regulates lysosomal biology in leukemia cells. INPP4B overexpressing (A) and INPP4B knockout (B) OCI-AML2 cells were labelled with 1uM lysotracker red were imaged by microscopy and quantitated using flow cytometry. INPP4B overexpressing (C) and INPP4B knockout (D) OCI-AML2 cells were labelled with Magic Red-cathepsin B were imaged by microscopy and quantitated using flow cytometry. Scale bar: 15 μm. E. Inducible-INPP4B OCI-AML2 cells were treated without or with doxycycline (100mg/mL) and incubated with DQ-BSA-Green™ and fluorescence was monitored by flow cytometry hourly, for up to 6 hours. Representative flow cytometry histograms displayed. F. Inpp4b+/+ and Inpp4B-/- MLL-AF9 leukemia blasts were incubated with DQ-BSA-Green™ and fluorescence was monitored by flow cytometry hourly, for up to 8 hours. Representative flow cytometry histograms displayed. G. Inpp4b+/+ and Inpp4B-/- MLL-AF9 leukemia blasts were plated in the LFC assay in the presence of Lys05 at indicated dose for 7 days and monitored for total colony counts or (H) percentage of type I and type II colonies. Inpp4b+/+ MLL-AF9 leukemia blasts were plated in the LFC assay in the presence of Lys05 at indicated dose for 7 days. Data represent + SEM from at least three independent triplicate experiments with at least 10,000 events per condition. Students t-test or ANOVA and post-hoc analysis are displayed with *P < 0.05, ** P < 0.01, *** P < 0.001, **** P < 0.0001 compared to indicated control condition.

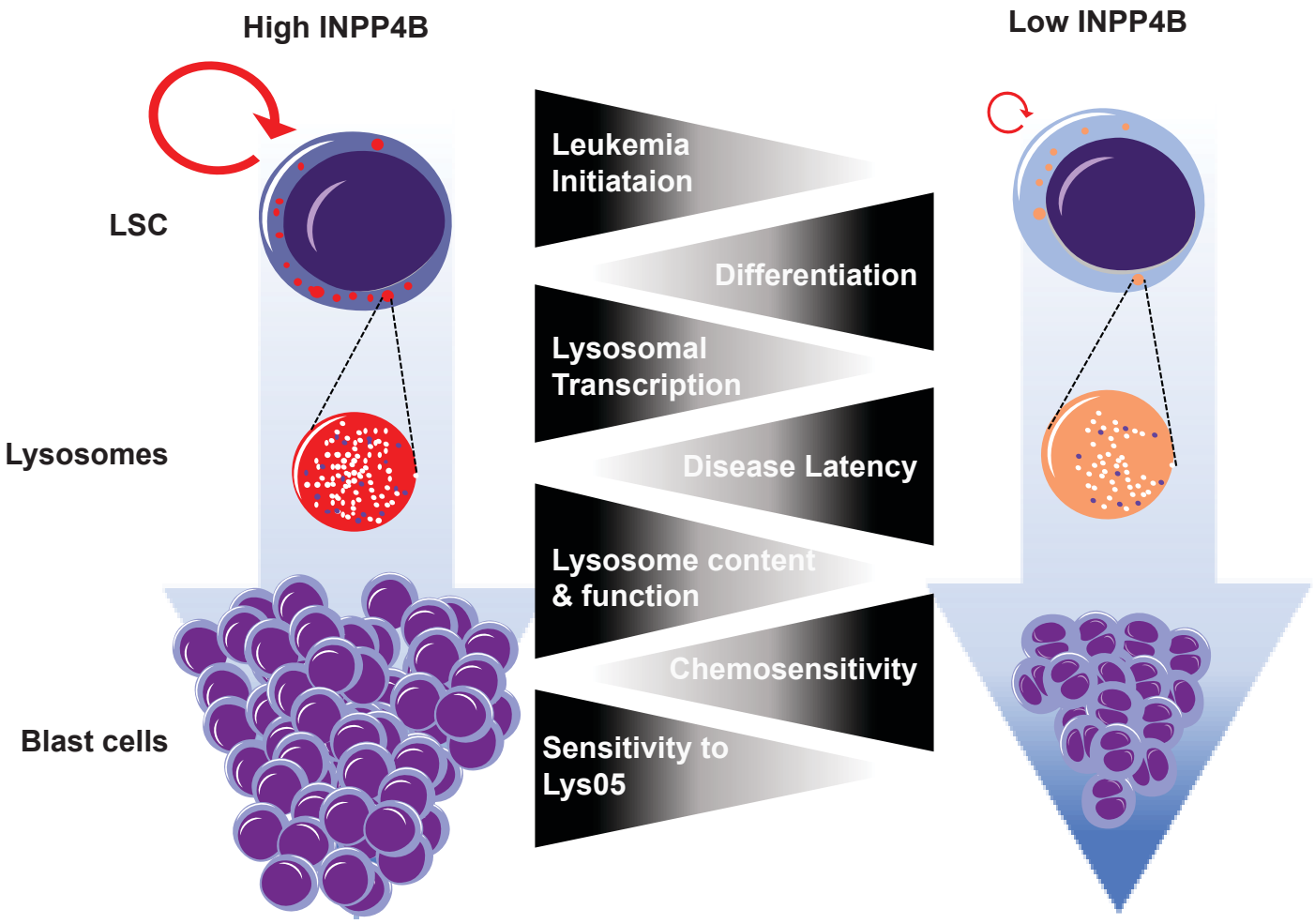

Figure 8: Model of INPP4B function in leukemia stem cells and leukemic blasts.